Journal of Building Engineering 84 (2024) 108501

Contents lists available at ScienceDirect

Journal of Building Engineering

journal homepage: www.elsevier.com/locate/jobe

Effect of raw materials on the performance of 3D printing geopolymer: A review

Kailun Chen [a,b], Qiong Liu [c], Bing Chen [d], Shishun Zhang [e], Liberato Ferrara [f], Wengui Li [a,b,*]

[a] Centre for Infrastructure Engineering and Safety, School of Civil and Environmental Engineering, The University of New South Wales, NSW, 2052, Australia
[b] School of Civil and Environmental Engineering, University of Technology Sydney, NSW, 2007, Australia
[c] School of Environment and Architecture, University of Shanghai for Science and Technology, Shanghai, 200093, China
[d] Department of Civil Engineering, Shanghai Jiao Tong University, Shanghai, 200240, China
[e] School of Civil and Hydraulic Engineering, Huazhong University of Science and Technology, Wuhan, 430074, China
[f] Department of Civil and Environmental Engineering, Politecnico di Milano, Piazza Leonardo da Vinci 32, Milano, Italy

ARTICLE INFO

Keywords:
Geopolymer composite
3D printing concrete
Life-cycle assessment
Low-carbon emission
Energy consumption

ABSTRACT

Traditional construction materials such as cement products release a significant amount of carbon dioxide during their preparation and usage, negatively impacting on the environment. In contrast, 3D printing (3DP) with geopolymer materials utilises renewable and low-carbon emission raw materials. It also exhibits characteristics such as energy efficiency and resource-efficient utilisation, contributing to reduction in carbon emissions and an improvement in sustainability. Therefore, the development of 3DP geopolymer holds great significance. This paper provides a comprehensive review of 3DP geopolymer systems, examining the effect of raw materials on processability, including flowability and thixotropy, and microstructure. The study also delves into sustainability and environmental impact. The evaluation highlights the crucial role of silicon, aluminium, and calcium content in the silicate raw material, influencing the gel structure and microstructural development of the geopolymer. Aluminium promotes reaction rate, increases reaction degree, and aids in product formation. Silicon enhances the mechanical properties of geopolymer, while calcium facilitates the formation and stability of the three-dimensional network structure, further improving material strength and stability. Moreover, the reactivity of raw materials is a key factor affecting interlayer bonding and interface mechanical properties. Finally, considering sustainability, the selection of raw materials is crucial in reducing carbon emissions, energy consumption, and costs. Compared to Portland cement, 3DP geopolymer material demonstrate lower carbon emissions, energy consumption, and costs, thus making it a sustainable material.

List of abbreviations

OPC	Ordinary Portland Cement
P_{st}	Slurry Pressure

* Corresponding author. School of Civil and Environmental Engineering, The University of New South Wales, NSW, 2052, Australia.
E-mail address: Wengui.li@unsw.edu.au (W. Li).

https://doi.org/10.1016/j.jobe.2024.108501
Received 8 November 2023; Received in revised form 13 December 2023; Accepted 9 January 2024
Available online 10 January 2024

σ_{cf}	Wall Friction Force
FA	Fly Ash
GB	Ground Brick Waste
HA	Halloysite
SS	Sodium Silicate
KSC	Kenaf Straw Core
KF	Kenaf Fiber
GGBS	Ground Granulated Blast Furnace Slag
SF	Silica Fume
SS	Steel Slag
FGD	Flue Gas Desulfurization Gypsum
C–S–H	Calcium Silicate Hydrate
C-A-S-H	Calcium Alumino-Silicate Hydrate
N-A-S-H	Sodium Alumino-Silicate Hydrate
(N,C)-A-S-H	Calcium Sodium Aluminate Silicate Hydrate
CDW	Construction Demolition Waste
HB	Hollow Brick
RCB	Red Clay Brick
RT	Roof Tile
CR	Concrete Rubble
CW	Concrete Waste
GW	Glass Waste
RH	Rice Husk
I_c	Composite Cost Index
PVC	Polyvinyl Chloride

1. Introduction

The 3D printing construction technology is an advanced building manufacturing technique. Typically, it uses concrete as the raw material and utilizes 3D printing equipment to stack it layer by layer. Through control systems and design programs, it gradually forms architectural components or entire buildings with complex geometries and internal structures. Compared to traditional construction processes, the advantages of 3D printing construction technology lie in its ability to achieve highly customized architectural designs without the need for templates. This reduces material waste and construction time, making the process environmentally friendly. Secondly, the printing process requires minimal human intervention, reducing construction waste and labor consumption while

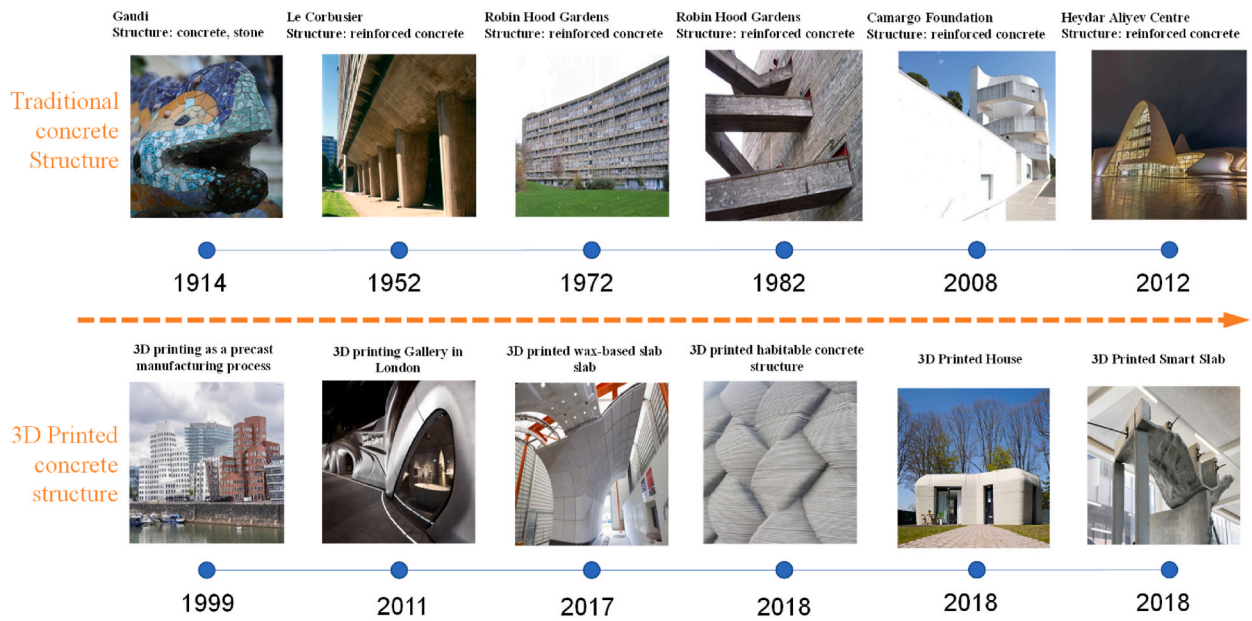

Fig. 1. Comparison of traditional building structures and structural applications of 3D printing construction technology [1].

increasing construction efficiency and safety. Furthermore, it enables the realization of complex internal structures and cavity systems, providing improved mechanical and energy performance. In addition, compared to traditional construction, this technology aligns with the principles of green construction and sustainable development, making it one of the most promising directions for the current building industry. Although the application of 3D printing technology in the field of construction is still in the exploratory and developmental stages, significant achievements have already been made in some actual engineering projects, as shown in Fig. 1.

This technology typically requires the use of specially designed 3D printers and concrete materials, where the concrete is often mixed with other additives and reinforcement materials additive manufacturing to improve its flow, printability, and strength [2,3]. However, geopolymer exhibits good plasticity under suitable humidity and viscosity conditions, making it suitable to produce complex shapes and structures using 3D printing technology. The plasticity of geopolymer enables the realization of architectural structures with unique designs and personalized requirements through 3D printing technology. Therefore, integrating geopolymer into 3D printing can offer advantages such as sustainability, resource availability, natural plasticity, low cost, and rapid construction.

Geopolymer, first discovered by Davidovits, is an amorphous inorganic material that is formed through a geopolymerisation reaction involving a source of silico-aluminates (such as clay or industrial waste) and an alkaline metal silicate solution at room temperature or below 100 °C [4]. Geopolymer is a polymer material with a specific chemical structure, where the polymer chains contain cross-linkable functional groups. It undergoes cross-linking reactions through alkaline activators, forming a network structure as shown in Fig. 2, which imparts it with excellent physical and chemical properties. These materials exhibit several desirable characteristics compared to Ordinary Portland Cement (OPC), including physicochemical stability, high durability, acid resistance, good thermal and heat stability, high mechanical performance, low CO_2 emissions, and low energy consumption [5]. There are the wide range of experiments of geopolymers in soil reinforcement, groundwater containment, and geohazard management in recent years [6–13].

On the other hand, the environmental pollution caused by cement has always been a significant concern. As shown in Fig. 3, according to data from STATISTA, global cement production has been increasing annually from 1995 to 2022. Particularly, in 2022, China accounted for 64 % of the global cement production, making it the largest cement-producing country in the world. However, due to the continuous growth of the global population, especially in developing countries and emerging markets, the increase in population has led to a demand for housing, infrastructure, and social services. Additionally, the processes of urbanization and industrialization have driven rapid development in infrastructure, residential, and commercial buildings. Moreover, developing countries and emerging markets are undergoing rapid urbanization and industrialization, requiring a significant amount of cement for construction and infrastructure expansion. Therefore, the demand for cement remains high across various countries globally. According to a survey conducted by On Field Investment Research, the cement demand in different countries worldwide in 2022 is depicted in Fig. 4.

There is no doubt that the Portland cement industry is an energy-intensive industry, in which the use of fossil fuels and carbon dioxide generated during clinker calcination is one of the major sources of greenhouse gas (GHG) emissions. CO_2 emissions from cement production contribute directly to the greenhouse effect and exacerbate the problem of global warming. It is estimated that cement production accounts for about 8–10 % of global CO_2 emissions [17]. In addition, according to STATISTA data, as shown in Fig. 5, China and India are the largest CO_2 emitters in the cement manufacturing industry worldwide. Therefore, there is a need to find some effective ways to reduce CO_2 emissions, and low carbon emission geopolymers are considered to be one of the best alternatives to cement in the future.

The combination of 3D printing technology and geopolymers has recently gained increasing attention as it holds promising implications for the sustainable development strategies in the construction industry. However, existing 3D printing technologies need to adapt to the unique properties and requirements of geopolymers. Due to the rheological and curing characteristics of geopolymers that may differ from traditional printing materials, it is necessary to conduct a comprehensive literature review on the current state of geopolymer behaviour in 3D printed materials for architectural applications. In the field of 3D printed buildings, one of the current major challenges is the limited range of available printing materials and the potential for improvement in their performance. Worldwide, the energy crisis is becoming increasingly severe, and concepts such as “low-carbon development", “industrial waste recycling", and “circular development" have become global consensus for development. Compared to the high carbon emissions in the cement manufacturing process, geopolymers offer lower carbon dioxide emissions during production. The use of geopolymers can reduce reliance on finite natural resources while minimizing negative environmental impacts. Geopolymers, which utilize waste or natural minerals as raw materials, contribute to lowering the carbon footprint of the construction industry and promoting sustainable development.

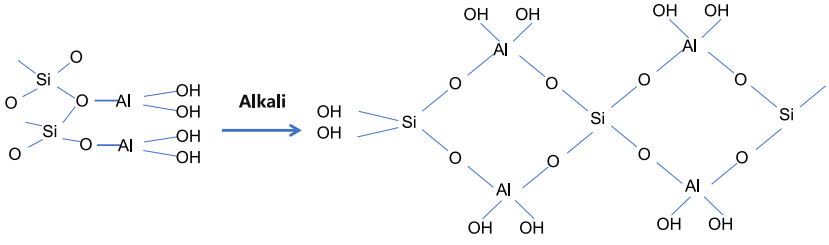

Fig. 2. Geopolymer reaction: polycondensation under alkaline exciters.

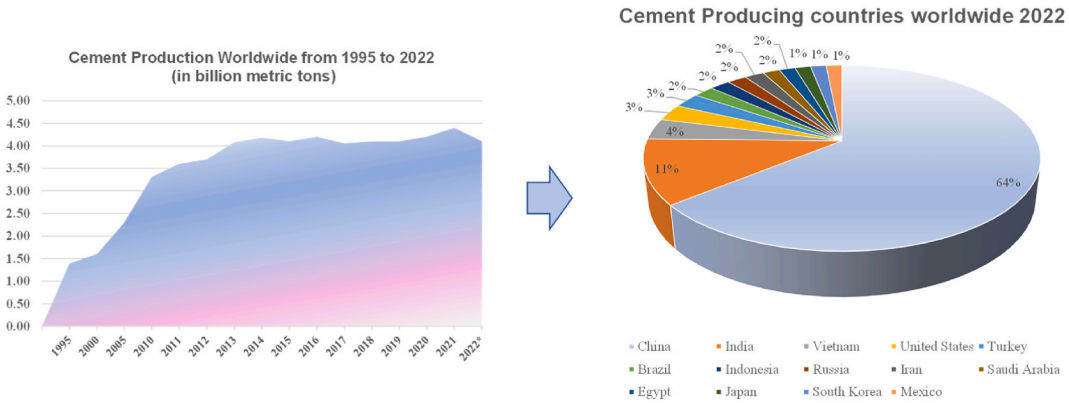

Fig. 3. Changes in global cement production from 1995 to 2022 and the share of cement production in different countries in 2022 [14,15].

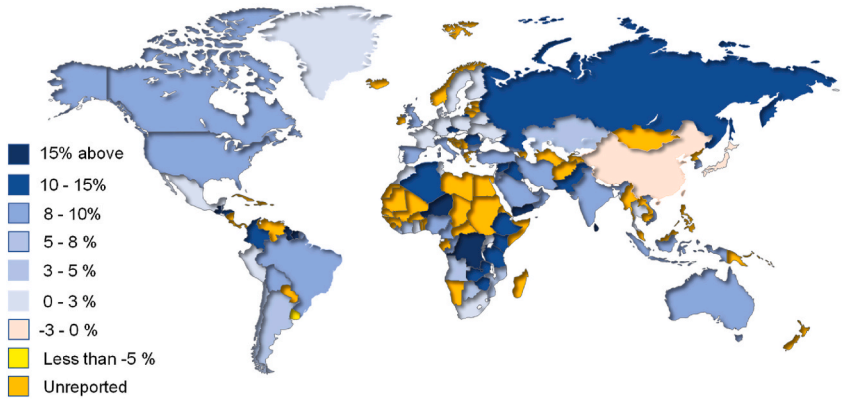

Fig. 4. Global demands for cement by country in 2022 [16].

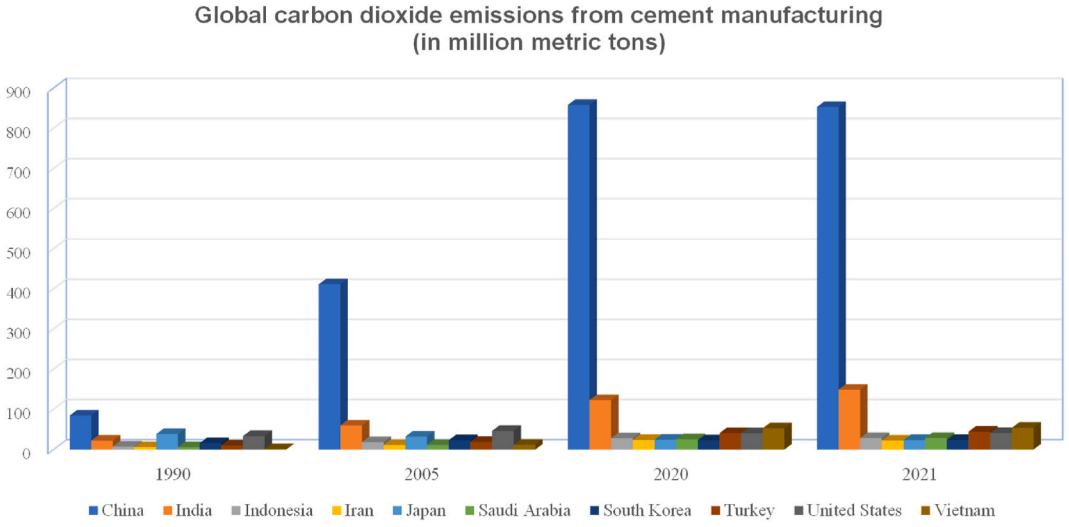

Fig. 5. Carbon dioxide from cement manufacturing in different countries [18].

Compared to OPC, geopolymer materials are promising candidates for 3D printing due to several advantages [19–22]. In terms of performance, geopolymers exhibit higher strength and durability, meeting the requirements of the 3D printing process. Economically, geopolymer materials often utilize industrial waste as their raw materials, resulting in lower costs. In terms of design, geopolymers can be prepared in various shapes and sizes, accommodating different design needs. They can be poured, sprayed, or molded into specific

shapes, enabling flexibility in architectural design. In summary, the combination of 3D printing technology and geopolymers holds potential for advancing sustainable development in the construction industry. Geopolymers offer advantages such as reduced environmental impact, lower carbon emissions, efficient resource utilization, and design flexibility, making them a promising choice as 3D printing materials in architectural applications.

This paper provides a comprehensive review of 3D printed geopolymer printing systems, the impact of raw materials on workability (which includes fluidity and thixotropy), microstructure, etc. It also provides an in-depth study of sustainability and environmental impacts: it evaluates the environmental friendliness of 3D printed geopolymers, the sustainability effects and the economic costs of synthesizing geopolymers using different raw materials and discusses the life cycle analysis and environmental friendliness of geopolymers.

2. 3D-printed geopolymer systems

The 3D printed geopolymer is a special type of material that can be used for actual creation using only a 3D printer. Since 3D printing does not require traditional techniques, such as building templates and vibration, 3D printed geopolymers have the advantage of being flexible, customizable, cost-saving and time-economical. The 3D printed slurry system is shown in Fig. 6. The 3D printed slurry system can be used for the creation of the 3D printed geopolymer. To ensure the implementation of this technology, its first step requires the use of computer-aided design software to create or obtain the build path of the geopolymer. In addition, during the printing process, it is necessary to monitor the print quality and ensure the stability of the model. Print speed, temperature and other parameters are adjusted to ensure that the geopolymer slurry is properly cured and attached.

On the other hand, the hopper has importance in the 3D printing system, as it provides a centralized supply of slurry, manages the flow of material, controls the environmental conditions of the material, and has replaceable and cleanable properties. As shown in Fig. 7, it is composed of a cylinder and a funnel, where the funnel shape is designed for easy flow of slurry. The hollow cylinder is designed with two inlets. The large feeding port is open for feeding, checking, and cleaning. The small feeding port is connected to the pipe, which can continuously feed the printing slurry into the hopper. In addition, another inlet can be opened on the surface of the hopper to deliver liquid accelerant into the hopper. The mixing of the liquid accelerant with the mortar in the hopper greatly improves the workability of the printing process slurry and does not change its pumpability during transportation.

However, due to the special characteristics of geopolymer slurries, this can lead to a number of problems when applying geopolymer slurries to 3D printing systems: firstly, for flowability, the rheological properties of geopolymer slurries may change over time, which may affect the material homogeneity and the stability of the printing process; poor particle dispersion can lead to clogging or inhomogeneous material flow during the printing process, thus affecting the quality of the prints; moreover, the viscosity of geopolymer slurries is critical for the success of the mixing and the printing process. Geopolymers with appropriate binders and activators can develop fast yield strength immediately after the initial contact between binder and activator, while at high shear mixing these mixtures exhibit low viscosity for pumping through nozzles, which remains low only for a short time after shear [25,26].

After that time, the slurry will develop excessive viscosity, which may lead to poor flow and printing difficulties. Therefore, to solve this difficulty, Muthukrishnan et al. [27] have developed a 3D printing system for geopolymer slurries, as shown in Fig. 8. The raw material and activator are transported to the hopper separately through different feed pipes, which can avoid the inconvenience caused by the initial mixing, for example, some silica-aluminate materials will appear agglomerate-like as well as overly viscous slurry after mixing with alkaline activator, which will reduce the printing efficiency. Therefore, with this system, the raw materials can be effectively kept in an inactivated state to improve the constructability of the printing process.

On the other hand, research into aggregate concrete 3D printing technology has gained popularity due to the need for large-volume construction materials. Compared to extrusion-based 3D printing technology, it can construct concrete structures with greater efficiency, making it ideal for large-scale construction projects that require a substantial number of concrete structures. The system

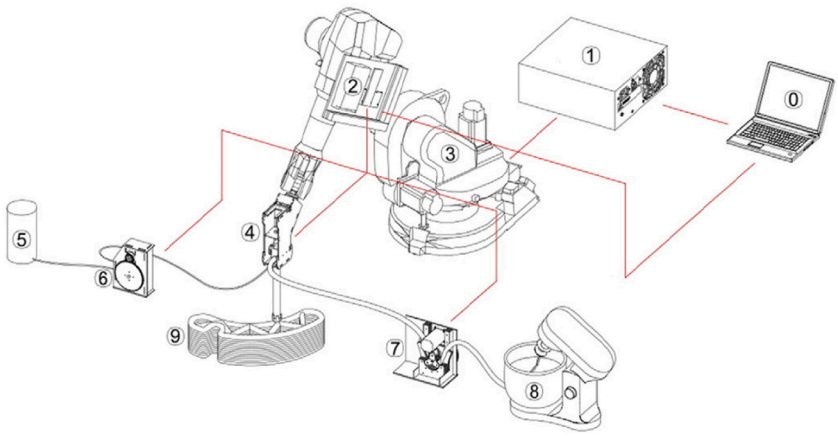

Fig. 6. Schematic diagram of the 3D printing (3DP) setup: 0. System commands; 1. Robot controller; 2. Print controller; 3. Robotic arm; 4. Print head; 5. Promoter; 6. Peristaltic pump for coagulant promoter; 7. Peristaltic pump for premixing; 8. Pre-mixing mixer; 9.3D printed object [23].

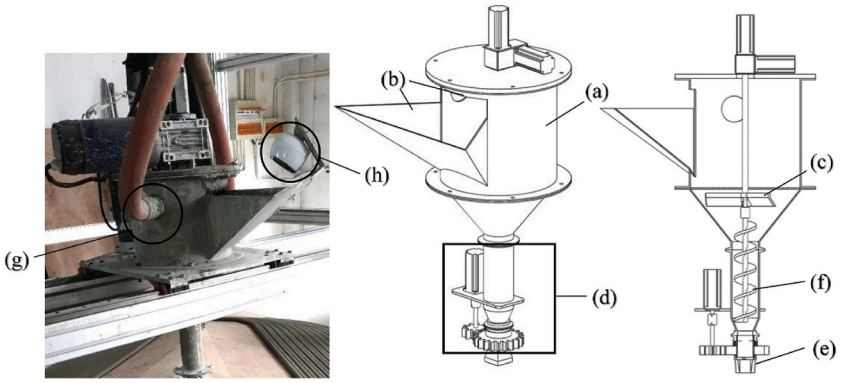

Fig. 7. Hopper and Slurry Extrusion Systems: (a) Hopper; (b) Feeding inlets; (c) Agitator; (d) Rotating mechanism; (e) Nozzle; (f) Screw; (g) Continuous feeding from small inlet through pipeline; (h) Monitor [24].

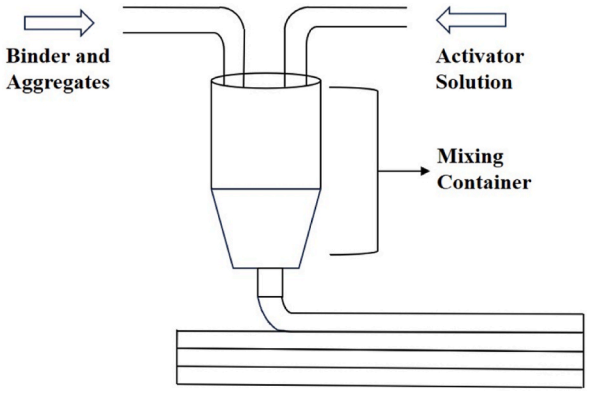

Fig. 8. Schematic representation of extrusion system for 3D printed geopolymers [27].

comprises three essential components: an aggregate feeder, paste feeder and blade, as demonstrated in Fig. 9. The integration of these supplementary devices enables flexibility in managing aggregate uncertainty and guarantees reliable control of concrete height for each layer. What's more, this approach facilitates separating the deposition of aggregates from cement or binder application. Compared to the direct mixing of aggregates and binders (e.g. cement) in the hopper, this separation method allows the introduction of different binder materials after the deposition of aggregates has been completed, providing greater flexibility and the possibility of varying material properties or compositions [28,29]. It should be noted that optimal rheological properties of the slurry are essential in aggregate bed methods to boost the quality of printed works. The flow of the slurry is a crucial factor in the printing process and affects the formation of the structure. Proper fluidity promotes adhesion between the layers and allows for quality structure formation. Conversely, if the slurry lacks fluidity, it may result in weak bonding between layers, negatively impacting the stability and strength of the structure. Moreover, the favorable rheological characteristics of the slurry can facilitate a homogeneous dispersion of particles within the bed layer, which is pivotal for achieving uniformity in structure during the printing procedure [28,30,31].

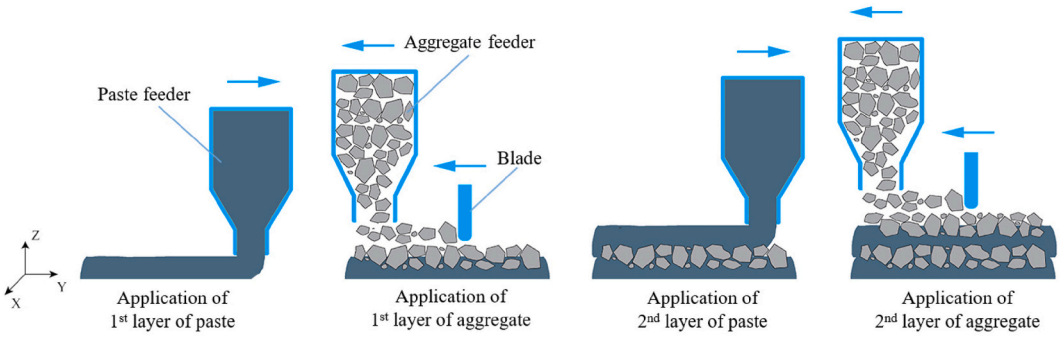

Fig. 9. Schematic representation of aggregated-bed 3D concrete printing process [32].

In the 3D printing process of geopolymers, the nozzle is a crucial component, as its size and shape have a significant impact on print resolution and detail. A smaller nozzle diameter can achieve higher print resolution and enable the printing of finer details and curves. Since some geopolymer products may contain complex shapes and details, selecting the appropriate nozzle size and shape is essential. Additionally, the geometry and size of the nozzle play a vital role in controlling the flow and speed of the geopolymer slurry. By adjusting the nozzle's diameter and outlet shape, the extrusion speed and volume of the geopolymer slurry can be controlled. This helps ensure stable extrusion of the geopolymer slurry, maintains a continuous printing flow, and avoids issues such as clogging and uneven material flow.

Muthukrishnan et al. [33] conducted a detailed study on the nozzles of 3D printing systems, as shown in Fig. 10, in which it was shown that in terms of fluid flow through the nozzles, the extrusion resistance should consist of four aspects: firstly, wall friction is generated as the paste moves towards the nozzles [34]. This force is caused by the contact between the slurry and the inner wall of the nozzle. This contact results in frictional resistance between the fluid and the wall surface, impeding the flow of the fluid. The magnitude of the frictional force is closely related to the roughness of the inner wall and the overall feed length. If the inner wall of the nozzle is rough or the feed length is long, the frictional force will increase, thereby increasing the extrusion resistance. Additionally, if necessary for experimental purposes, additional molds are often installed in the nozzle, which introduces additional frictional forces acting on the inner surface of the mold [34,35]. Finally, during the extrusion process, a forming zone is formed near the nozzle exit. In this zone, two types of resistance are encountered: the slurry pressure (P_{st}) and the wall friction force (σ_{cf}) within the conical region. The intensity of these resistances depends on the cone angle (θ) of the conical region. The P_{st} refers to the pressure exerted by the fluid within the forming zone. When the slurry is forced through the nozzle, it exerts pressure on the surrounding walls, resulting in flow resistance.

On the other hand, the σ_{cf} is the frictional force between the slurry and the inner wall of the conical region. This force occurs due to the contact between the fluid and the wall surface, adding to the resistance of fluid flow. The magnitudes of the slurry pressure and the wall friction force are influenced by the θ of the conical region. A larger cone angle leads to greater slurry pressure and wall friction force, resulting in increased resistance during the extrusion process. In summary, the forming zone near the nozzle exit experiences two types of resistance: slurry pressure and wall friction force. The intensity of these resistances is determined by the cone angle of the conical region [33,36,37]. Overall, wall friction is an important factor affecting the extrusion resistance of a fluid through a 3D printing system nozzle. Therefore, there is a need to optimize the nozzle design to minimize wall friction to improve the performance and printability of the 3D printing system.

To achieve the desired shape and good buildability required for 3D printing, it is essential to have a suitable nozzle. Various nozzle shapes have been used as orifices for extrusion machines, including circular, elliptical, square, and rectangular shapes, as shown in Table 1. Choosing the right nozzle shape depends on several factors, such as the desired printing resolution, the material being extruded, and the specific requirements of the printing process. Each nozzle shape has its advantages and limitations. Circular nozzles are commonly used and offer a simple and versatile design. They provide consistent extrusion and are suitable for a wide range of materials. However, they may not be ideal for achieving intricate details or sharp edges. Elliptical nozzles enable better control over the material flow and can be advantageous for applications that require precise and adjustable extrusion widths. They can provide better resolution and finer details compared to circular nozzles. Square and rectangular nozzles are often used for applications that require precise layer deposition, such as in the construction industry. They can help in achieving straighter lines and smoother surfaces, especially for larger-scale prints. It is important to note that nozzle shape is only one aspect of the overall printing system. Other factors, such as nozzle diameter, print speed and extrusion speed, also play a crucial role in achieving the desired print results.

In the 3D printing of geopolymers, side wipers can also be used at the nozzle orifice to achieve a better surface finish, as shown in Fig. 11. A side wiper is a thin plate or surface installed next to the nozzle orifice, which is used to smooth or scrape the surface of the extruded material. It helps remove any irregularities or protrusions in the extruded material, thereby improving the surface quality of the print. The benefits of using side wipers include: 1. This can improve surface smoothness where side wipers can help flatten the surface of the extruded material, reducing or eliminating layer lines or raised features that may occur during the printing process; 2. It also can enhance printing precision, which side wipers enable control over the extruded material during the printing process, ensuring uniform filling of each printed layer; 3. This would increase material adhesion where side wipers can provide additional force to

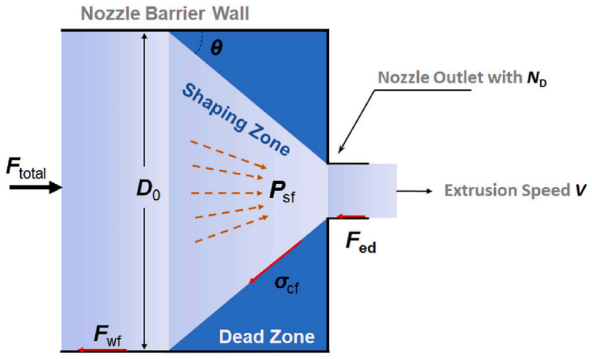

Fig. 10. Simplified diagrams of the force on the slurry through the nozzle [33].

Table 1
Printing characteristics of different nozzle sizes.

Nozzle shape	Dimension (mm)	Extrusion speed (L/min)	Printing speed (mm/s)	Nozzle lifting height (mm)	Refs.
Orbicular	20		20	10	[38]
Orbicular	3.5		30	5	[39]
Rectangular	20 × 4		5	20	[40]
Orbicular	30	0.5	10	30	[41]
Orbicular	15		50	9	[42]
Rectangular	30 × 20	1.6	44	20	[43]
Rectangular	10 × 20	3	150		[44]
Slice			60	30	[45]

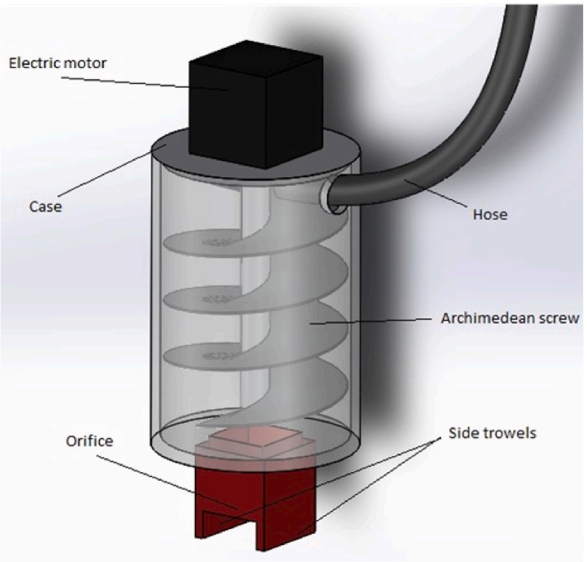

Fig. 11. Spray set assembly with side scrapers [48].

improve the adhesion of the extruded material to the print bed or the previous layer [46–50].

Generally, a circular nozzle provides high degrees of freedom in 3D printing and does not require adjusting the printing angle. However, in rapid printing of complex structures, the small contact area between layers or beads may affect the constructability or stability of the layers. Previous research has indicated that square-shaped nozzles resulted in better surface smoothness compared to elliptical nozzles and were easier to manufacture [48]. Additionally, the nozzle size depends on the size and shape of the object being printed. Currently, as shown in Table 1, the size range for 3D printing rectangular and circular nozzles is 10 × 20 mm to 30 × 20 mm and 3.5–30 mm, respectively, but this does not mean the nozzle sizes are limited to these ranges. The design of existing nozzles allows

Table 2
Effect of raw materials on coagulation properties of 3D printed geopolymer slurries.

Items	Raw materials	Sample preparation	Setting time (min)	Refs.
Halloysite reinforced 3D-printable geopolymers	Halloysite (HA), Fly Ash (FA)	FA + HA + Sand + Alkali (Sodium Silicate (SS) + NaOH)	400–720	[51]
3D concrete printing of eco-friendly geopolymer containing brick waste	Ground Brick waste (GB), Slag, FA	GB + Slag + FA + Alkali (Sodium Metasilicate) + Retarder + Nano clay	102–168	[52]
Kenaf Stalk geopolymer on printability and performance of 3D print	Kenaf Straw Core (KSC), Kenaf Fiber (KF), Ground Granulated Blast furnace Slag (GGBS), FA	KSC + KF + GGBS + FA + Alkali (SS + NaOH)	57–216	[53]
The effects of Nano-additives in strengthening mechanical performance of 3D printed geopolymer	FA, GGBS, Silica Fume (SF)	FA + GGBS + SF + Alkali (SS + NaOH)	Less than 60	[38]
3D printed geopolymer only with water	Slag, FA	FA + Slag + Sand + Alkali (SS + Anhydrous Sodium Metasilicate) + Retarder	55-more than 480	[54]
3D concrete printing of geopolymer with quaternary binders	GGBS, FA, Steel Slag (SS), and Flue Gas desulfurization Gypsum (FGD)	Slag + FA + SS + FGD + Sand + Alkali (SS)	75–180	[42]

for nozzle sizes and printing speeds within the range of 5–150 mm/s. In summary, when it comes to 3D printing geopolymers, nozzle design needs to be taken into consideration as it can impact print quality, accuracy, and flowability, among other factors. Furthermore, Zhang et al. [33] suggest that nozzle design should aim to reduce extrusion resistance to achieve good printing quality.

3. Effect of raw material on workability

3.1. Setting time

The setting time can influence the rheological properties and shape retention of the printed geopolymer after being extruded from the print head. If the time is too short, the geopolymer slurry may not have enough time to maintain the desired shape during the printing process, leading to a decrease in geometric and dimensional accuracy of the printed structure. Adequate time ensures sufficient solidification of the geopolymer material during the printing process, resulting in good bonding and internal structure formation. In short, the solidification time is directly related to the speed and efficiency of 3D printing geopolymers. Shorter that time can accelerate the printing speed, enabling faster production and improved efficiency. However, previous research has shown significant variations in that time due to the differences in raw materials for geopolymers, as demonstrated in Table 2.

Ranjbar et al. [51] found in their study on HA-enhanced 3D geopolymer concrete that increasing the content of HA reduced the setting time of the slurry. Typically, it is widely believed that adding inert materials increases the solid-to-liquid ratio, providing more surface area for the precipitation of reaction products, which should shorten the setting time of the geopolymer matrix. However, the improvement in the specific surface area of the inert precursor did not affect the overall setting time, attributed to the higher specific surface area of HA leading to an increase in reactivity, thereby accelerating the geopolymerisation process. Pasupathy et al. [52] stated that the setting time of fresh mixtures for 3D geopolymer concrete prepared from waste bricks increased with increasing brick waste content. This was primarily due to the lower reactivity of the components in the brick waste and the slower rate of geopolymerisation. Waste bricks typically contain silica and other silicate materials, which participate in the geopolymerisation reaction. However, compared to other raw materials, waste bricks exhibit lower reactivity, resulting in a relatively slow geopolymerisation rate. This means that in mixtures containing a higher proportion of waste bricks, it takes more time for the geopolymerisation reaction to fully occur, leading to an increase in the setting time. Kong et al. [53] suggested that using recycled sand with a high-water absorption rate could accelerate the reaction rate, leading to higher strength in 3D printing samples. On the other hand, the addition of red hemp stalks helped to shorten the setting time of the material. The high-water absorption capacity of the recycled sand allowed for better water distribution within the mixture, promoting effective hydration of the cementitious materials. This results in the formation of a denser and stronger geopolymer matrix, thereby improving strength properties. In addition, red hemp stalks contained organic additives that acted as accelerators for the geopolymerisation reaction. These organic compounds enhance the reactivity of the geopolymer precursors, thereby speeding up the geopolymerisation rate. As a result, the setting time of the material is reduced, allowing for quicker hardening, and achieving early strength development. Overall, the use of high-absorption recycled sand and the addition of red hemp stalks can accelerate the hydration rate and geopolymerisation process in 3D printing, leading to higher strength. The high-water absorption of the recycled sand improves water distribution, while the organic additives in red hemp stalks act as accelerators for geopolymerisation. This shortens the setting time of the material, enabling faster hardening and early strength development.

Lemougna et al. [55] showed that increasing the content of slag, which was the main source of calcium, had a significant effect on the slurry setting time. By increasing the content of slag, more calcium ions could be supplied to accelerate the process of calcium silicate formation, which in turn accelerated the slurry setting time. In addition, the fine particles and surface area in slag also helped to accelerate the coagulation process. Slag typically has a large specific surface area, providing more reactive interfaces that facilitate the reaction. This increased reaction surface area promotes the formation of gelling products and accelerates the coagulation time. Similarly, Chougan et al. [38] discovered in their study on nano-reinforced 3D printed geopolymer that a high dosage of slag in the geopolymer helped in forming a denser structure, leading to a rapid setting time. This was primarily attributed to the increased content of CaO in the mixture due to the higher slag content. The elevated CaO content facilitated the formation of Calcium Silicate Hydrate (C–S–H) gel through early geopolymerisation reactions and the development of a 3D stable silico-aluminate structure.

The above-mentioned research indicates that the physical properties of the raw materials, such as the solid ratio of inert materials, and their chemical composition significantly impact the setting time of 3D printed geopolymer materials. The chemical composition of the reactive mixture has a significant influence on the geopolymerisation reaction because it defines the degree of geopolymerisation in the silicate solution. The setting time of the geopolymer mixture is also determined by the presence of alkaline substances in the solution. Solutions with a high content of M − O (M represents alkaline cations such as Si, Al, etc.) species exhibit a shorter setting time for geopolymer mixtures, indicating a higher degree of geopolymerisation in the solution. In other words, a high concentration of M − O species corresponds to a high degree of depolymerization. Depolymerized species have a small volume and high reactivity, enabling them to rapidly form oligomers, thereby affecting the setting time [55–63].

In short, such as the solid ratio of inert materials, and the chemical composition of the raw materials significantly influence the setting time of 3D printed geopolymer materials. The chemical composition of the reactive mixture plays a crucial role in the geopolymerisation reaction by determining the degree of geopolymerisation in the silicate solution. The presence of alkaline substances in the solution affects the setting time of the geopolymer mixture. Solutions with a higher content of M − O species exhibit a shorter setting time, indicating a higher degree of geopolymerisation. A higher concentration of M − O species corresponds to a higher degree of depolymerization, which results in smaller volume depolymerized species with stronger reactivity, enabling the rapid formation of oligomers and influencing the setting time. In addition, in terms of the physical properties of the raw materials, increasing the solids ratio of inert materials also reduces the solidification time; and materials with a high-water absorption rate can also speed up the reaction process.

3.2. Effect of raw materials on thixotropic properties

Thixotropy is the ability of a material to deform reversibly, after being subjected to force or shear. In the case of 3D printed geopolymer materials, thixotropy can have a definite impact on the printing process and results. As shown in Fig. 12, in the 3D printing process, the molding of slurry often requires sufficient yield strength between the layers to be molded, and the stability of a single layer is usually required to reach a yield strength of 180–1000 Pa, and the bottom layer needs to reach a yield strength of approximately 12 KPa to cast a 1 m structural frame [64]. Therefore, designing and having good thixotropy improves the material's shear resistance at low shear rates while ensuring that the material maintains its structure and shape under self-weight and upper gravity, as well as good bonding between the printed layers, in other words thixotropy contributes to the printability and stacking performance of 3D printed geopolymer pastes.

However, raw materials have an important influence on the thixotropy of 3D printed geopolymers. The thixotropy is usually determined by the rheological properties and components of the material. Guo et al. [65] prepared 3D printed FA-based geopolymers using FA and quartz sand as raw materials, and slag powder and silica fume as auxiliary gelling materials. From Fig. 13, thixotropic experiments revealed that a moderate content of slag powder (10 %) was very beneficial to the thixotropy of the geopolymer slurry. This was mainly attributed to the enhancement of plastic viscosity, containing a large number of silicon, aluminum, calcium elements of slag, FA and SF can be with the liquid phase of hydroxide ions occurring in the geopolymerisation reaction to generate gelling products, such as C–S–H, Calcium Alumino-Silicate (C-A-S-H), etc., which were conducive to improving the plastic viscosity of the slurry, thus having a better thixotropy.

In their study on the effect of bentonite on 3D printed composites, Chen et al. [66] found that as shown in Fig. 14, the area of the hysteresis curve gradually increased from 10802 Pa/s to 17380 Pa/s when the bentonite content was gradually increased from 0 to 3 %, which implied that bentonite could effectively improve the thixotropy of 3D printed composites. This was mainly attributed to the high-water absorption of bentonite and that it could form a flocculated structure in the liquid phase, resulting in higher shear stress. When secondary shear was applied, this leads to structural disruption and hydrogen bond breaking due to the formation of hydrogen bonds and flocculent structures within the particles, thus the study further suggested that thixotropy existed where the rate of bond breaking was greater than the rate of the reconstruction process.

Zhou et al. [67] investigated the effect of bauxite tailings on the rheological behaviour of 3D printed composites, as shown in Fig. 15, and found that the shear stress in the ascending stage was significantly greater than that in the descending stage at the same shear rate, resulting in the formation of hysteresis curves, which implied that a large number of gelled products were formed in the early stage of the slurry, which required a high shear stress to destroy the structure, and then in the descending stage, due to the destruction of the structure of the gelled lattice leading to the reduction of friction in the slurry. Reduction of friction within the slurry due to the destruction of the cementitious grid structure during the descent phase. Therefore, it could be concluded that bauxite tailings contributed to the thixotropy of the slurry, which is also due to the high reactivity of bauxite tailings.

Rheological measurements of fresh geopolymer are crucial for predicting the printability of the mixture. However, different raw materials have a significant impact on the 3D printing slurry. Geopolymers are essentially suspensions of liquid-solid dispersions, and their rheological properties are largely influenced by interparticle colloid and inertial contact, particle solubility, and viscous interactions with alkaline agents. It is worth noting that the elemental composition of the silico-aluminate precursor has been shown to play a crucial role in controlling the rheological behaviour of geopolymer [56,68–76]. In general, silico-aluminate materials with volcanic ash activity can generate a large amount of gelling material under the action of alkaline activators, forming flocculent or grid-like structures that require higher shear stress to break down. In the descending stage of the shear process, the flocculent or grid-like structures of the gel product are disrupted as the shear rate increases, resulting in the formation of many free particles that have not participated in the reaction and smaller flocculated structures. Compared to the ascending stage, this effect can reduce the internal friction of the slurry, resulting in lower shear stress at the same shear rate.

On the other hand, the printability of geopolymers in 3D printing is greatly influenced by thixotropy. The thixotropic properties of geopolymers are also significantly affected by the selection and combination of raw materials, such as those with high levels of alumina and silica, as well as alkaline activators and additives. Finely ground particles with a narrow size distribution tend to enhance

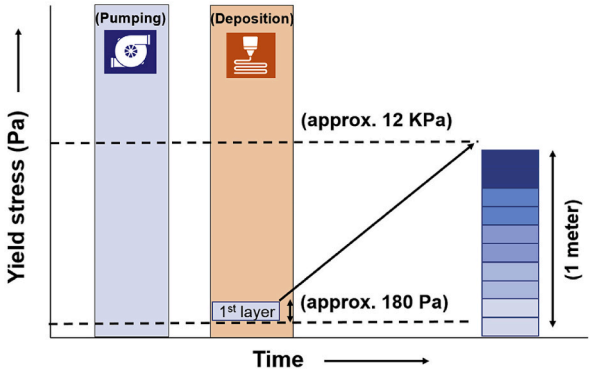

Fig. 12. Plot of bottom yield strength against height [64].

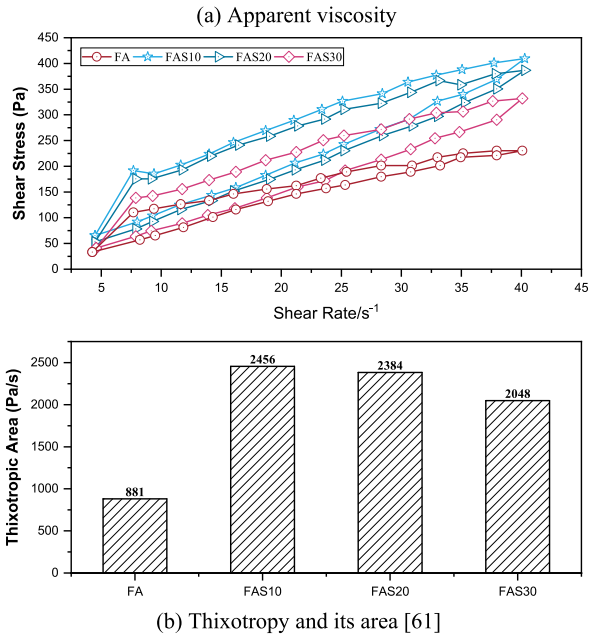

Fig. 13. The influence of content of slag powder on the rheological properties on fly ash-based matrix geopolymers (a) Apparent viscosity (b) Thixotropy and its area [65].

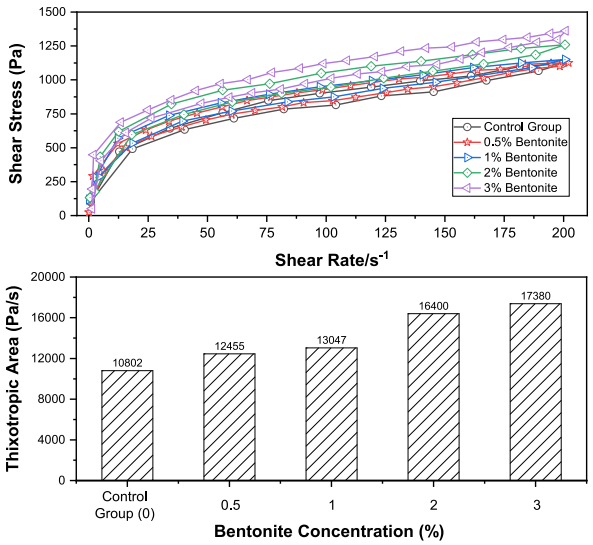

Fig. 14. Effects of bentonite content on the thixotropy of composite slurries: Thixotropy and its area [66].

thixotropy, which promotes better flow and shear thinning properties. The thixotropic behaviour of geopolymers is affected by the distribution and physical properties of solid particles. Additionally, the type and concentration of alkali activator also have an impact on the thixotropic properties of geopolymers. Geopolymers with appropriate thixotropic properties display shear-thinning properties which reduce viscosity when extruded or deposited, thus aiding fluid passage through the printer nozzle and enhancing layer-by-layer deposition for improved printability. Furthermore, good thixotropy assists in interlayer adhesion and structural stability.

4. Effect of raw materials on mechanical properties

The importance of mechanical performance for 3D printed geopolymer is self-evident. The mechanical properties of the geopolymer slurry have a significant impact on the structural integrity and stability of the printed object. Mechanical performance indicators such as strength and stiffness determine the resistance to deformation and fracture of the printed object under load. Better mechanical performance ensures that the printed object can withstand the effects of external forces and environmental factors, thereby

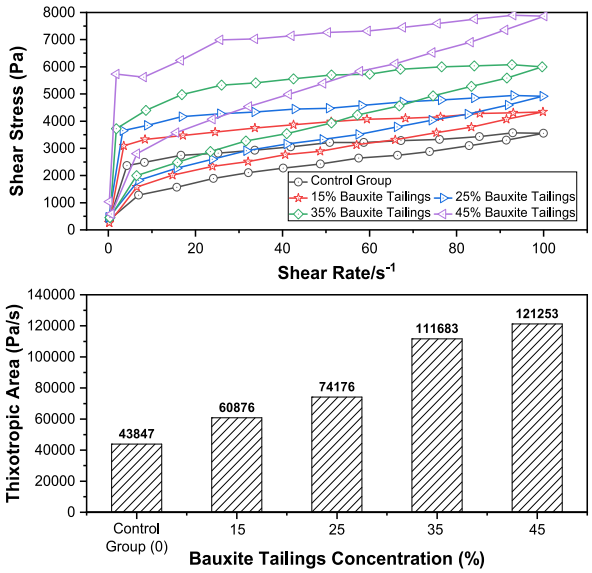

Fig. 15. The influence tailings content on rheological behaviours: Thixotropy and its area [67].

maintaining its geometric shape, dimensions, and performance stability. The choice of raw materials is one of the important factors affecting the mechanical performance of 3D printed geopolymer. Different raw materials can have a significant impact on the strength, toughness, hardness, and other mechanical properties of the printed object. By properly combining different raw materials, the mechanical performance of geopolymer samples can be significantly improved. For example, raw materials with higher reactivity such as slag can significantly enhance the strength and stiffness of geopolymer prints. Nano-fillers or microsphere fillers can improve wear resistance and impact resistance, among other properties.

Table 3 lists the mechanical properties of 3D printed geopolymer in recent years. From the table, the compressive strength of geopolymer slurry after 28 days of curing ranges from 20 MPa to 56.8 MPa, and some samples even achieve a strength of 75 MPa in just 7 days. However, the flexural strength is not ideal. From the results of the raw material composition and mechanical strength, it is not difficult to see those raw materials with higher reactivity, such as silica-alumina materials like slag and SF, can significantly improve the compressive strength of geopolymer prints. Additionally, nano-fillers like nano-clay, with their larger specific surface area and reinforcement effect, can be uniformly dispersed in the geopolymer matrix to increase the hardness and strength of the printed objects.

It is worth mentioning that at the level of printed specimens, Biranchi Panda et al. [78] showed that the compressive strength of geopolymer-printed samples exhibited strength similar to that of cast samples, which was attributed to the fact that the well-designed printing process prevented the formation of voids during the extrusion of the mixture. However, a contrary view was presented by Hau Bong and Wolfs et al. [54,83]. They stated that the compressive strength of the printed samples was 10–27 % lower than that of the molded samples, which was attributed to the higher apparent porosity of the printed samples compared to the cast samples, which inevitably introduces some voids between the layers during the layer-by-layer stacking process, resulting in a lower degree of densification. Therefore, the printing process requires careful consideration of the rheological properties of the printed material and a well-designed printing process.

For raw materials, in an investigation [64] it was found that the compressive strength of samples containing nano-clay was reduced by about 17 %. In general, the use of 0–3% nano-clay is effective in improving geopolymer samples, which is related to the space-filling ability of nano-clay to densify the microstructure of the samples. However, since the clays used in this experiment were inherently hydrophilic, they may have led to some water adsorption, which slowed down the reaction of the geopolymer, resulting in lower mechanical properties. Hussam Alghamdi et al. [79] found that due to the presence of high levels of reactive silica in the slag, this led to an increase in the volume and structure of the reaction products, which could effectively improve the compressive strength of samples; however, the high content of slag samples performed poorly in flexural strength tests, which was mainly attributed to the fact that the high shrinkage of the slag-containing alkali activation caused a large number of microcracks, which led to the flexural strength being poorer (Microcracks had a greater effect on flexural strength than on compressive strength). Similarly, Mehdi Chougan et al. [38] found that higher doses of slag in 3D printed geopolymer samples helped to increase the C-A-S-H and Sodium Alumino-Silicate (N-A-S-H) content, which resulted in the formation of a denser structure for higher strengths; furthermore, the incorporation of nano-additives and SF helped to form an underlayer with a well-compacted base layer, which led to an increased loading capacity of the underlayer, resulting in a higher bending strength in the vertical direction.

Ilcan et al. [80] demonstrated in their study that construction demolition waste (CDW), which included materials such as hollow bricks, red clay bricks, roof tiles, glass, and concrete rubble, tended to have low available silicon content. In the initial stage, dissolved $Ca2+$ ions tended to react with the available Si in the medium, forming gel products that promote strength development. However, during the geopolymerisation process, the availability of dissolved Si ions in the medium might be limited. As the particle dissolution

Table 3
Mechanical strength of 3D printed geopolymers prepared from different raw materials.

Major elements	Combination method	Compressive strength	Flexural strength	Refs.
FA: SiO_2 (49.10 %), Al_2O_3 (39.35 %), Fe_2O_3 (3.48 %) SF: Not available GGBS: Not available	FA + GGBS + SF + sand + activator	36 MPa (28 days)	5.05 MPa (28 days)	[77]
FA: SiO_2 (49.15 %), Al_2O_3 (39.35 %), CaO (2.94 %) GGBS: SiO_2 (29.65 %), Al_2O_3 (15.56 %), CaO (39.37 %) SF: SiO_2 (98.37 %), Al_2O_3 (0.19 %), CaO (0.35 %)	FA + GGBS + SF + sand + activator	18.4 MPa (7 days)		[78]
FA: SiO_2 (51.1 %), Al_2O_3 (28.8 %), CaO (5.8 %) GGBS: SiO_2 (29.60 %), Al_2O_3 (15.50 %), CaO (39.30 %) Nano-clay: SiO_2 (65.30 %), Al_2O_3 (15.04 %), CaO (2.26 %)	FA + GGBS + Nano-clay + activator	20–35 MPa (28 days)		[64]
FA: SiO_2 (58.40 %), Al_2O_3 (23.80 %), CaO (7.32 %) GGBS: SiO_2 (36.0 %), Al_2O_3 (10.5 %), CaO (39.8 %) Cement: SiO_2 (19.60 %), Al_2O_3 (4.09 %), CaO (63.21 %) Limestone (L): $CaCO_3 > 99$ % Alumina powder (A): $Al_2O_3 > 99$ %	FA + GGBS + Cement + activator + L + A	5–38 MPa (28 days)	1–5.5 MPa (28 days)	[79]
FA: SiO_2 (52.18 %), Al_2O_3 (24.16 %), CaO (3.47 %) GGBS: SiO_2 (33.06 %), Al_2O_3 (10.34 %), CaO (45.29 %) SF: SiO_2 (98.37 %), Al_2O_3 (0.19 %), CaO (0.35 %)	FA + GGBS + SF + Nano-graphite platelets + sand + activator	35–75 MPa (7 days)	7–12 MPa (7 days)	[38]
FA: SiO_2 (56.74 %), Al_2O_3 (24.89 %), CaO (5.20 %) GGBS: SiO_2 (32.19 %), Al_2O_3 (12.53 %), CaO (43.23 %)	FA + GGBS + sand + activator + water	33–56.8 MPa (28 days)	3.5–8.4 MPa (28 days)	[54]
Hollow Brick (HB): SiO_2 (39.7 %), Al_2O_3 (13.8 %), CaO (11.6 %) Red Clay Brick (RCB): SiO_2(41.7 %), Al_2O_3(17.3 %), CaO (7.7 %) Roof Tile (RT): SiO_2 (42.6 %), Al_2O_3(15.0 %), CaO(10.7 %) Glass (G): SiO_2 (66.5 %), Al_2O_3 (0.9 %), CaO (10.0 %) Concrete Rubble (CR): SiO_2 (31.6 %), Al_2O_3(4.8 %), CaO (31.3 %)	HB + RCB + RT + G + CR + activator	8–11 MPa (7 days) at binary activator 9–17 MPa (7 days) at ternary activator		[80]
HB: SiO_2 (39.7 %), Al_2O_3 (13.8 %), CaO (11.6 %) RCB: SiO_2 (41.7 %), Al_2O_3 (17.3 %), CaO (7.7 %) RT: SiO_2 (42.6 %), Al_2O_3 (15.0 %), CaO (10.7 %) Concrete Waste (CW): SiO_2 (31.6 %), Al_2O_3 (4.8 %), CaO (31.3 %) Glass Waste (GW): SiO_2 (66.5 %), Al_2O_3 (0.9 %), CaO (10.0 %)	HB + RCB + RT + GW + CW + activator	10–13 MPa (7 days) 14–16 MPa (28 days) 16–23 MPa (90 days)	2.5–5 MPa (7 days) 3–5.5 MPa (28 days) 3.5–6.5 MPa (90 days)	[81]
FA: SiO_2 (53.1 %), Al_2O_3 (20.5 %), CaO (6.3 %) HA: SiO_2 (54.1 %), Al_2O_3 (44.4 %), CaO (0.1 %)	FA + HA + sand + activator	2.5–4 MPa (3 days) 6–15 MPa (7 days) 27–40 MPa (28 days)	0.5–2 MPa (7days) 9–15 MPa (28days)	[51]
FA: SiO_2 (29.62 %), Al_2O_3 (15.75 %), CaO (25.97 %)	FA + sand + activator	15–16.5 MPa (3 days) 19–21 MPa (14 days) 23–25 MPa (28 days)		[82]

probability and the cation concentration of the alkali activator increase, repulsive forces between particles could occur. This process could limit the ion migration rate and result in the formation of heterogeneous regions composed of unreacted particles. Ultimately, this would lead to the formation of defects in the microstructure of the matrix, resulting in poor mechanical performance of the 3D printed geopolymer slurry prepared from CDW.

Overall, the compressive strength of 3D printed geopolymer can be influenced by the following factors: 1. Presence of reactive silica: if the raw materials contain highly soluble and reactive silica, such as slag, silica fume, and kaolin clay, increasing their content

can help stimulate or accelerate the geopolymerization reaction; 2. SiO_2/Al_2O_3 ratio: an increased that ratio promotes the formation of shorter and stronger Si–O–Si bonds compared to Si–O–Al and Al–O–Al bonds [84–86]. This results in stronger geopolymer bonds and a denser/harder microstructure rich in silica-alumina geopolymer gel [87,88]; 3. High CaO Content: A higher content of CaO in the raw

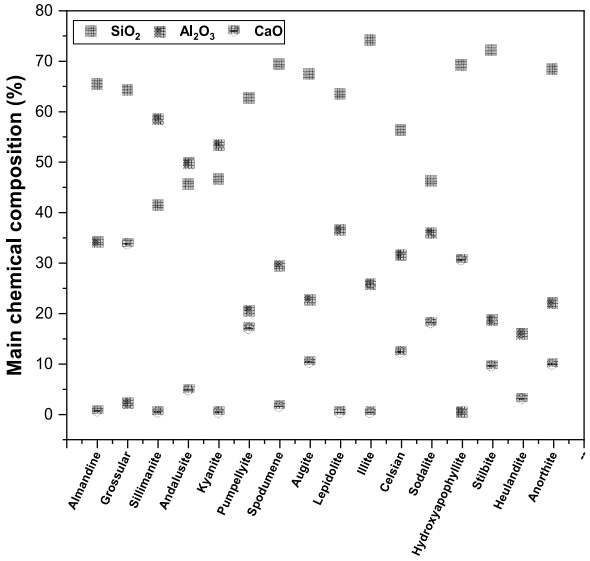

(a) Main chemical composition

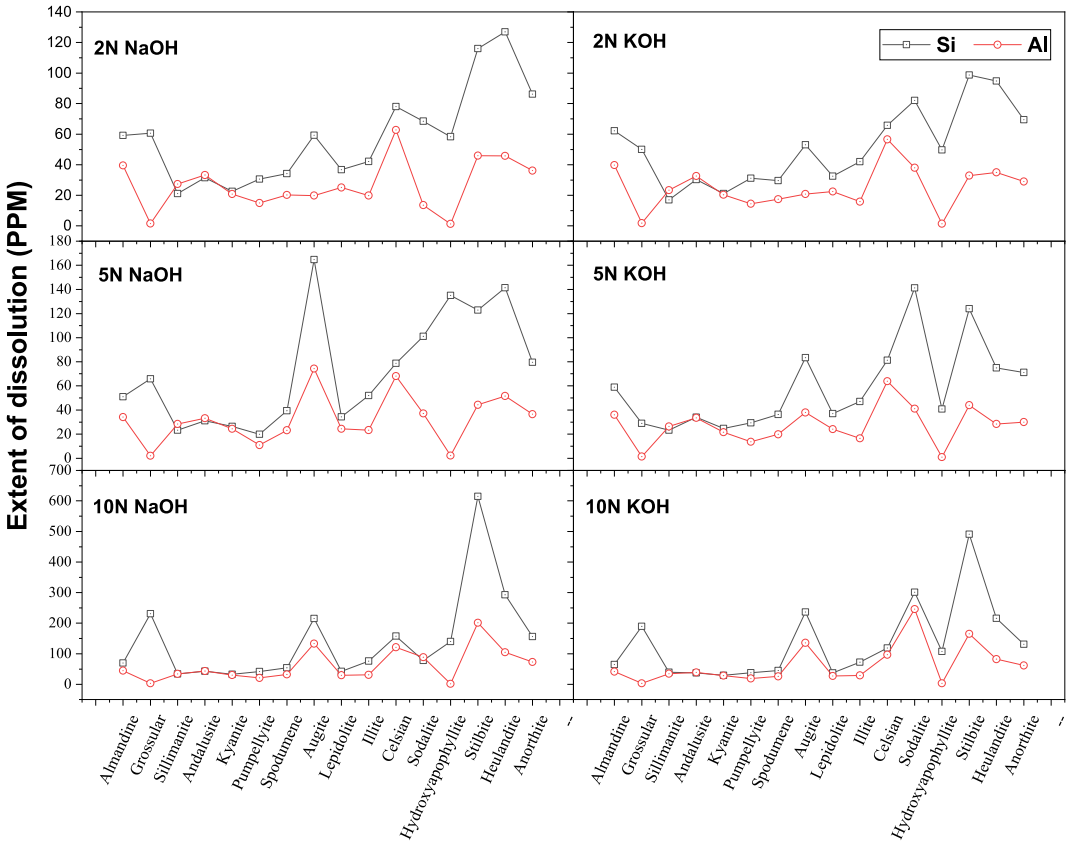

(b) Degree of Si and Al solubility (PPM)

Fig. 16. Degree of solubility of 16 minerals at two different concentrations of alkali [105].

materials can increase the pH value of the slurry and further activate the geopolymerisation reaction. Additionally, the elevated concentration of Ca^{2+} in the slurry system can lead to the initial formation of C–S–H gel, which can trigger higher initial strength [80]. Therefore, incorporating raw materials with high soluble reactive silica, increasing the SiO_2/Al_2O_3 ratio, and higher CaO content can contribute to enhancing the compressive strength of 3D printed geopolymer.

4.1. Alkaline activator

The importance of alkaline activators in 3D printed geopolymers for mechanical strength cannot be overlooked. They play a crucial role in the mechanical properties such as strength, hardness, and durability of geopolymer components. Firstly, the selection and concentration of the alkaline activator directly influence the rate and extent of the geopolymerisation reaction in the system. Proper selection and control of the type and concentration of the activator can achieve an appropriate curing reaction, providing sufficient strength to the geopolymer components during and after the printing process. Insufficient activator concentration may result in an incomplete reaction, leading to inadequate strength of the components.

On the other hand, excessive activator concentration can cause rapid reactions, resulting in unstable structures and lower mechanical strength [89–93]. Secondly, the influence of alkaline activators extends to the control of the microstructure of the specimens. By adjusting the type and content of the activator, it is possible to control the porosity, pore size, surface morphology, and other characteristics of the geopolymer components. These adjustments can have a significant impact on the final mechanical properties of the printed structures [94–98]. In addition, alkaline activators interact with other additives and admixtures, further influencing the mechanical strength of geopolymer components. For example, when used in combination with reinforcing fiber materials, the activator can promote the bonding between the fibers and the geopolymer matrix, thereby enhancing the strength and toughness of the components [99–103]. As a result, the proper selection, concentration, and interaction of alkaline activators in 3D printed geopolymer systems are critical for achieving desired mechanical properties and optimizing the performance of the printed structures.

The gel products closely related to mechanical strength ($nM_2O{\cdot}Al_2O_3{\cdot}xSiO_2{\cdot}yH_2O$ gel formed during the geopolymerisation process) depend on the dissolution of Si and Al in alkaline solutions [104]. Xu et al. [105] collected the concentrations of Al and Si after 5 h of contact between 20 ml solutions (including different concentrations of NaOH and KOH, 2 N, 5 N, and 10 N for both NaOH and KOH) and 0.5g minerals. Fig. 16 presents the dissolution data for all 16 minerals. Based on these data, the authors summarized the following trends: 1) mineral dissolution was positively correlated with alkaline solution concentration; 2) NaOH solution was more effective in mineral dissolution compared to KOH, except for nepheline; 3) overall, Si dissolved more than Al; 4) Si and Al exhibited synchronous dissolution behaviour in alkaline solutions; 5) minerals with a framework structure had higher dissolution extended in NaOH and KOH solutions compared to minerals with orthorhombic, cyclic, chain, and layered structures.

On the other hand, Xu et al. [107] suggested that the dosage of silico-aluminates materials depended on the particle size, dissolution extent, and concentration of the alkaline solution. Fine particles with a diameter less than 0.5 μm had higher dissolution extents, which allowed for the use of a relatively lower ratio of silico-aluminate powder to alkaline solution. This was because the majority of particles could undergo geopolymerisation to form gel products. However, in practice, most silico-aluminate particles did not undergo geopolymerisation smoothly. This might be attributed to various factors, such as the rapid formation of the gel products that could encase and hinder subsequent reactions, or the presence of inert protective layers on the particles, among other possibilities. Nevertheless, even though the geopolymer contains undissolved aluminosilicate solids, these particles can act as matrix reinforcement [108–110].

In summary, the dissolution of Si and Al in silico-aluminates materials is closely related to alkaline activators, and the dissolution of Si and Al has a direct impact on the formation of geopolymer products. Once silico-aluminates powder is mixed with alkaline solution, it forms a paste-like substance and rapidly transforms into a hardened geopolymer. In this case, it can prevent the 3D-printed geopolymer from forming a well-defined crystalline structure. Therefore, by selecting the correct type and concentration of alkaline activators, it can influence the speed and extent of the geopolymerisation reaction during the 3D printing process. Different types of

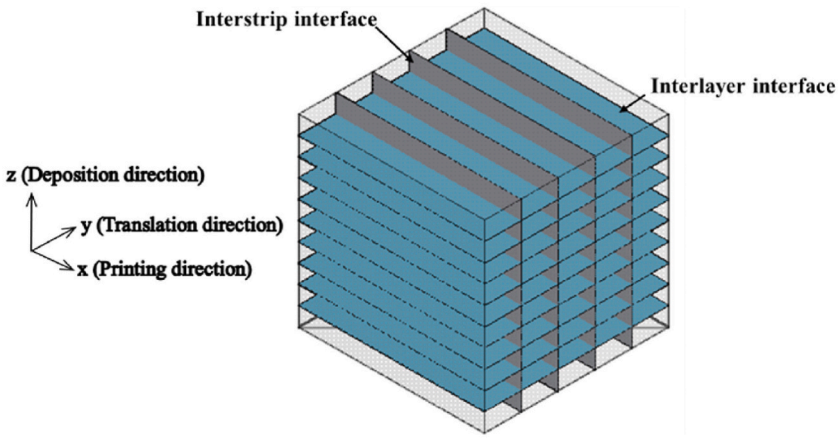

Fig. 17. Conceptual model of 3D printed slurry interlayer [106].

activators have distinct alkalinity and reaction properties, which can affect the formation and curing process of the geopolymer. By adjusting the activator concentration, it can control the reaction rate and physical properties of the geopolymer, thereby optimizing the performance of the printed components. This optimized mechanical strength is crucial for meeting the strength requirements in various application fields. In the construction industry, optimized polymer components can provide sufficient strength and durability to withstand structural loads and environmental impacts.

4.2. Interlayer bonding strength

The interlayer strength is crucial for the overall stability and quality of 3D-printed geopolymer objects. A strong interlayer connection ensures the structural stability of the printed model, preventing displacement and separation between layers. It also provides the mechanical strength and durability required for the printed object to withstand external stresses and loads; additionally, it can contribute to enhancing the fatigue resistance of the samples, allowing them to withstand long-term cyclic stresses [111–113]. The interlayer strength has a significant impact on the structural integrity, mechanical performance, fatigue resistance, and visual quality of 3D-printed geopolymer objects. It is essential for achieving high-quality and reliable printing results.

Previous studies have reported that due to the formation of bubbles during the mixing process of geopolymer slurry, 3D-printed geopolymer objects contained a significant number of interfaces (including interlayer and interstrip interfaces, as shown in Fig. 17) during the sequential layer stacking process. These interfaces often exhibit lower strength properties compared to cast samples. It has been proven that the performance of such interfaces significantly impacted the overall mechanical properties and durability of the samples. Weaker bonding forces between adjacent layers, as compared to cast structures, could lead to poorer structural integrity of the printed object [107,108]. Although the investigation of interlayer strength in 3D-printed geopolymer has become a hot and frontier topic in the academic community, systematic studies on its interface properties remain very limited so far.

Cagatay Demiral et al. [114], in their study, performed partial break tests on 3D-printed geopolymer samples. They placed the samples between compression plates and introduced a cylindrical metal rod at the junction of two consecutive layers, as shown in Fig. 18 (a). This allowed them to determine the maximum force required to separate the layers from each other. For direct tensile testing, a single-hole metal plate was fixed within the jaws of a tensile testing machine, and direct tensile stress was applied to the specimen, as illustrated in Fig. 18 (b).

The overall test results, as shown in Fig. 19, demonstrate a continuous strengthening of the tensile strength of the samples with increasing curing time, with maximum values of 1.35 and 1.79 MPa for splitting and direct tensile strength, respectively. Furthermore, the study found that the increase in alkali concentration had minimal impact on the interlayer strength test results compared to the mechanical performance test results. However, the interlayer strength is primarily influenced by the effective bonding area and the chemical and physical properties of the raw materials, with the raw materials having a greater influence. Raw materials with a high calcium content facilitate the production of more cementitious products, which can reduce the porosity within the matrix and improve the interface transition zone between the geopolymer slurry and aggregates.

On the other hand, Pasupathy et al. [52] used an apparatus as shown in Fig. 20 to measure the interlayer strength. The samples were clamped between metallic brackets at the top and bottom, and the tapered claws of the metal brackets were aligned with the interfaces of the sample's layers. This approach ensured a uniform distribution of interlayer stress and provided more accurate results compared to the method used by Cagatay Demiral et al. [114]. The tests were performed using a displacement-controlled mode at a rate of 1 mm/min. Additionally, small notches with a size of 4 mm were prepared at the interlayer region of the sample to ensure failure occurred at the interface of the 3D-printed filaments.

Fig. 21 shows the results of interlayer bond strength for 3D-printed samples with different levels of brick waste content. The inclusion of brick waste has a detrimental effect on the interlayer strength, meaning that an increase in the brick waste content reduces the interlayer bond strength of the samples. This can primarily be attributed to the higher content of brick waste replacing the desired mixture, which results in a significant presence of unreacted brick waste particles in the matrix. These unreacted particles lead to a weaker interlayer bonding, resulting in reduced interlayer strength.

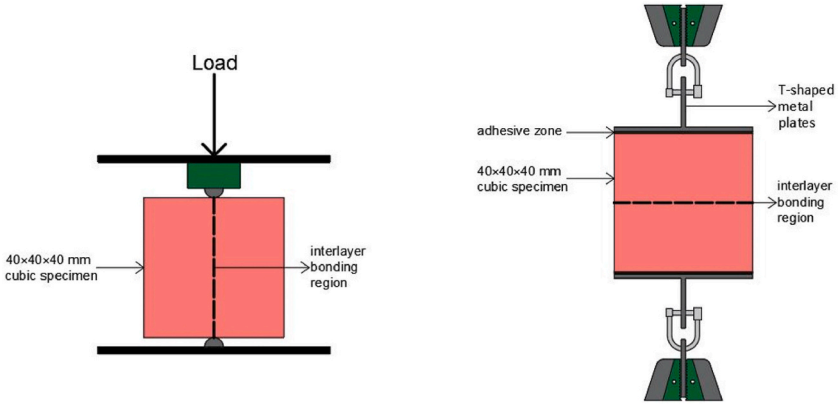

Fig. 18. Sketch of bond strength test: (a) splitting tensile strength and (b) direct tensile strength test [114].

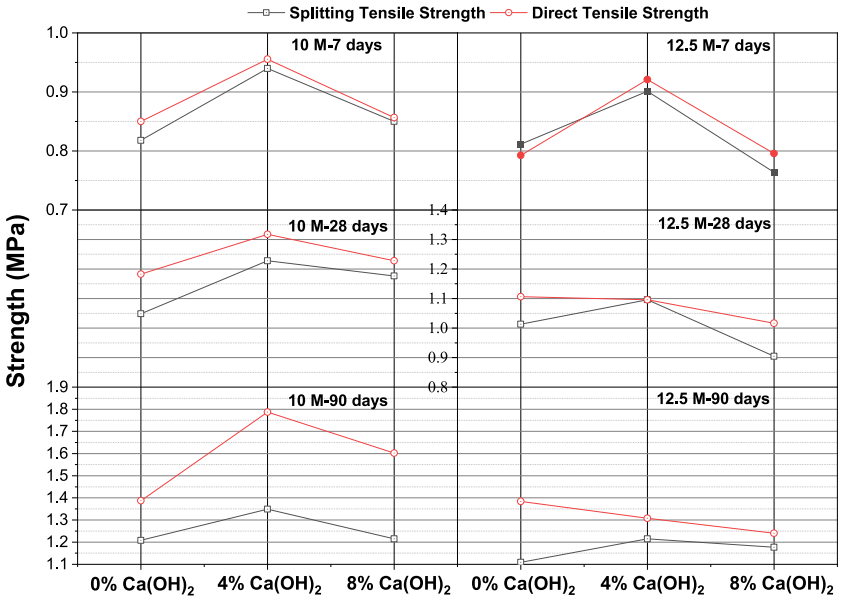

Fig. 19. Split strength and direct tensile strength test results [114].

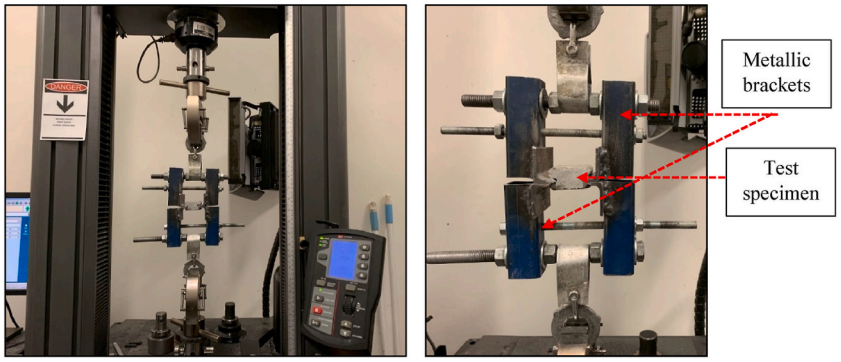

Fig. 20. Interlayer bond strength measurement [52].

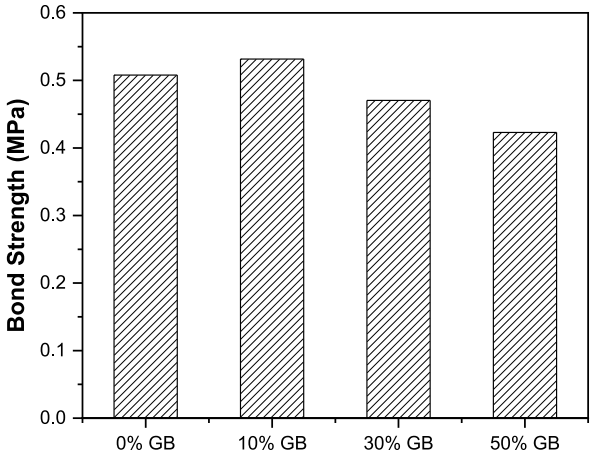

Fig. 21. Interlayer bond strength values of 3D printed samples [52].

Indeed, Keita et al. [115] pointed out that for low-porosity fresh materials (such as those with highly reactive raw materials that could form a low-porosity structure during the early stages of reaction), the internal moisture migration within the samples was hindered due to the dense structure. This led to certain areas not receiving an adequate supply of moisture during the sample's formation and curing process, resulting in the formation of dry regions within the sample. In these dry regions, there was insufficient water and gel products to fill the voids, thereby reducing the interfacial strength. This was because in a moist environment, water and gel products facilitate interfacial bonding and strengthening. However, in dry regions, the lack of these components adversely affected the interfacial strength. Therefore, ensuring an adequate water supply and uniform moisture migration is crucial for improving the interfacial strength of the samples, particularly when using highly reactive raw materials.

Furthermore, Moelich et al. [116] conducted a detailed study on the process of moisture variation between layers and simulated this process, as shown in Fig. 22. They identified four stages in the overall process: 1. Interconnection between aggregates, particles, and the pore fluid; 2. Formation of bleeding phenomena in the presence of gravity; 3. Liquid evaporation process; and 4. Gradual formation of a water-curved meniscus between solid particles, providing an opportunity for localized air permeation within the pore system. In addition to the physical process of water evaporation, the chemical process of geopolymerisation is also an essential part. During the chemical stage, the loss of water primarily occurs through geopolymerisation reactions and the formation of early gel products, such as C-A-S-H and C–S–H gels. These chemical reactions play a crucial role in the development of the geopolymer matrix, where the water loss is associated with the formation of gel-products, resulting in the hardening, and strengthening of the material. The formation of these gel products contributes to the interfacial bonding and the overall strength of the 3D-printed samples.

The main factors affecting the interlayer strength of 3D printed geopolymer can be categorized into chemical and physical factors. In terms of chemical factors, the reactivity of the raw materials is an important factor influencing interlayer bonding. Raw materials with higher reactivity can be a double-edged sword. Under the stimulation of alkaline agents, they can form more gelatinous products on the effective bonding zone and substrate, thus reducing the interlayer porosity and improving the interface transition zone. However, at the same time, these materials can form a dense structure in the early stages of reaction, inhibiting moisture migration and leading to dry regions and poor adhesion areas. Additionally, if the raw materials are inert or low-reactivity materials, such as CDW, there will be a significant number of unreacted particles in the interface region, resulting in a poor interlayer transition zone. On the other hand, for physical factors, the interface moisture field and moisture transfer are key factors influencing the mechanical properties of the interface.

However, most studies have not discussed the primary mechanisms behind the interlayer bonding strength of 3D printed geopolymers, whether they are of a physical or chemical nature. It is currently unclear whether the chemical or mechanical interface bonding mechanisms serve as the primary factors affecting the bonding strength. Furthermore, different interlayer drying, dehydration, and shrinkage can occur, significantly impacting the final interlayer bonding strength.

5. Effect of raw material on the microstructure

Raw materials serve as the foundation for the formation of the microstructure of 3D printed geopolymers. Factors such as molecular structure, particle shape, and reactivity of the raw materials directly impact the structure of the geopolymer. Different characteristics of the raw materials lead to changes in the microfeatures of the geopolymer. For instance, highly reactive particle raw materials often exhibit a granular structure [117,118]. When added to the geopolymer, they can fill the voids within the matrix. This filling effect alters the microstructure and increases its density.

Guo et al. [65] showed that 10 % slag powder was beneficial in modifying the microstructure of 3D printed fly ash-based geopolymers as shown in Fig. 23(a). The highly reactive slag powder was favorable to promote the formation of gel products in this system, constituting a dense microstructure, however, for the interlayer bonding region, a large number of unreacted fly ash particles with cracks were found in this region. Fig. 23(b) demonstrates a clearer picture of the interlayer microstructure. From the figure, obvious cracks were found to exist between the interfaces.

Similarly, Panda et al. [119] also observed the presence of silico-aluminate gel and unreacted FA and ground GGBS particles in the

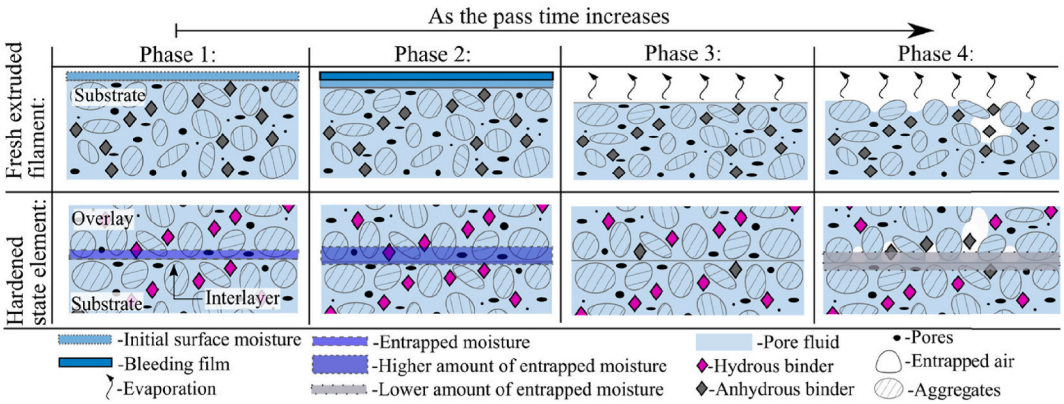

Fig. 22. Modeling of moisture variation in 3D printed interlayer structures [116].

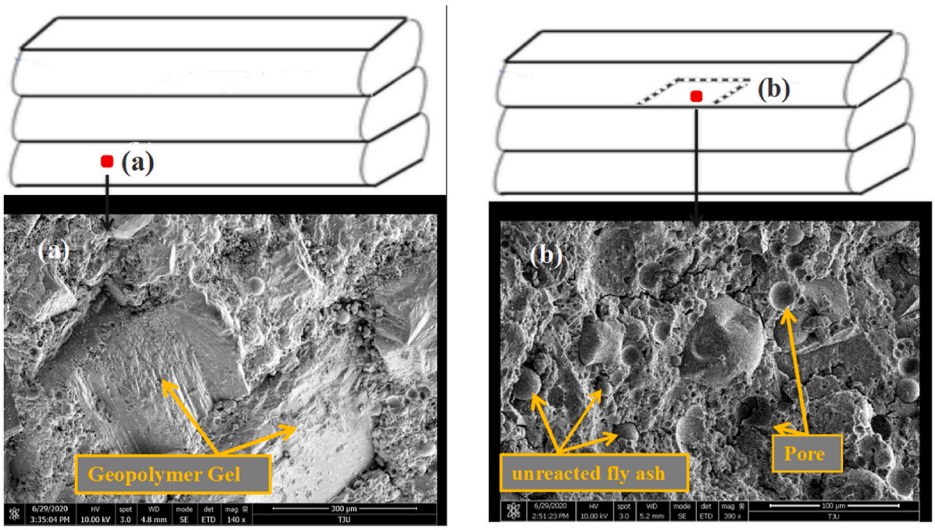

(a) The centre of a printed layer

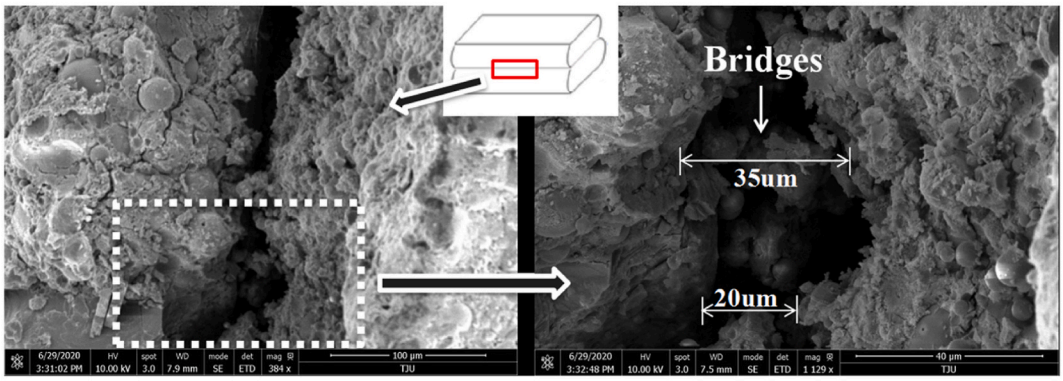

(b) Interlayer surface [61]

Fig. 23. Micro-characterization of 3D printed fly ash-based geopolymers: (a) Centre of a printed layer; (b) Interlayer surface [65].

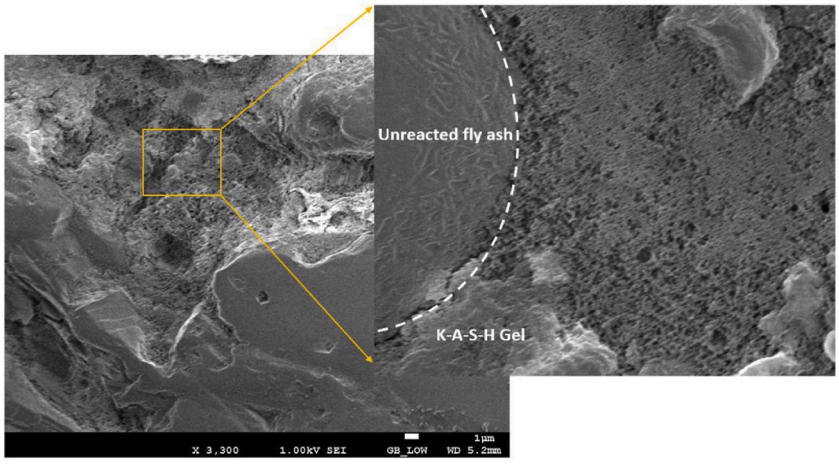

Fig. 24. The 3D printed fly ash-GGBS geopolymer microstructure after 28 days of curing [119].

microstructure of 3D printed FA-GGBS geopolymers, as shown in Fig. 24. The study suggests that the slag with a higher amorphous content (97.2 %) was the primary factor determining the dense microstructure, compared to the fly ash amorphous content (only 38.8 %). Previous research has also shown that amorphous materials, due to their inherent defects, exhibited higher reactivity, which facilitates the geopolymerisation reaction and led to the formation of more gel products [109].

On the other hand, Ranjbar et al. [51] demonstrated that low-reactivity HA, as a micro-filler and microfiber, remained in the hardened 3D printed FA geopolymer matrix, as shown in Fig. 25. In contrast, high-reactivity *meta*-halloysite dissolved during the reaction process and generated more gel products to fill the voids. Additionally, many unreacted FA particles could still be observed, either dispersed or filling various pores. It is evident that the reactivity of *meta*-halloysite is higher than that of HA and FA.

For low-reactivity materials, Pasupathy et al. [52] demonstrated that the addition of waste bricks had a detrimental effect on the microstructure of 3D printed FA-slag geopolymer, as shown in Fig. 26. Based on the microstructure images, Fig. 26(a) displayed a dense microstructure, indicating good compatibility between FA and slag, resulting in a well-formed microstructure. However, with the introduction of brick waste (10–50 %), a lower density and fragmented morphology could be observed, along with a significant presence of unreacted brick waste particles, as shown in Fig. 26(d).

In recent years, Sravanthi Puligilla et al. [120] have conducted in-depth research on the microstructure development of FA-slag geopolymers with respect to the role of slag. The results of their study indicated that the dissolution of calcium in slag determined the microstructure morphology of this binary geopolymer system. High-calcium content in the slag not only increased the reaction rate but also enhanced the extent of reaction and product formation. In particular, the presence of free calcium improved the rate and extent of FA particle dissolution, as well as the degree of product formation. Similar findings have been reported by other studies as well [121–123]. This highlights the important role of calcium dissolution in the microstructure development of FA-slag geopolymers. These research findings provide valuable insights into the formation mechanism and microstructure of FA-slag geopolymers. By controlling the dissolution process of calcium in slag, it is possible to regulate the reaction rate and extent of the geopolymerisation, thereby achieving the desired microstructure and properties.

On the other hand, for fiber-reinforced materials, Kong et al. [53] found a significant presence of N-A-S-H compounds and C–S–H gel in 3D printed FA-slag geopolymers, as shown in Fig. 27(a). When 1.5 % KSC were added, the fibrous KSC with a layered structure was surrounded by the geopolymer matrix, without noticeable gaps, as depicted in Fig. 27(b). Additionally, KSC retained its original form, indicating its function as a framework for supporting the specimen and maintaining its shape. However, its addition to the system increased the porosity of the geopolymer to some extent, which hinders the improvement of microstructural density. When 0.2 % KF

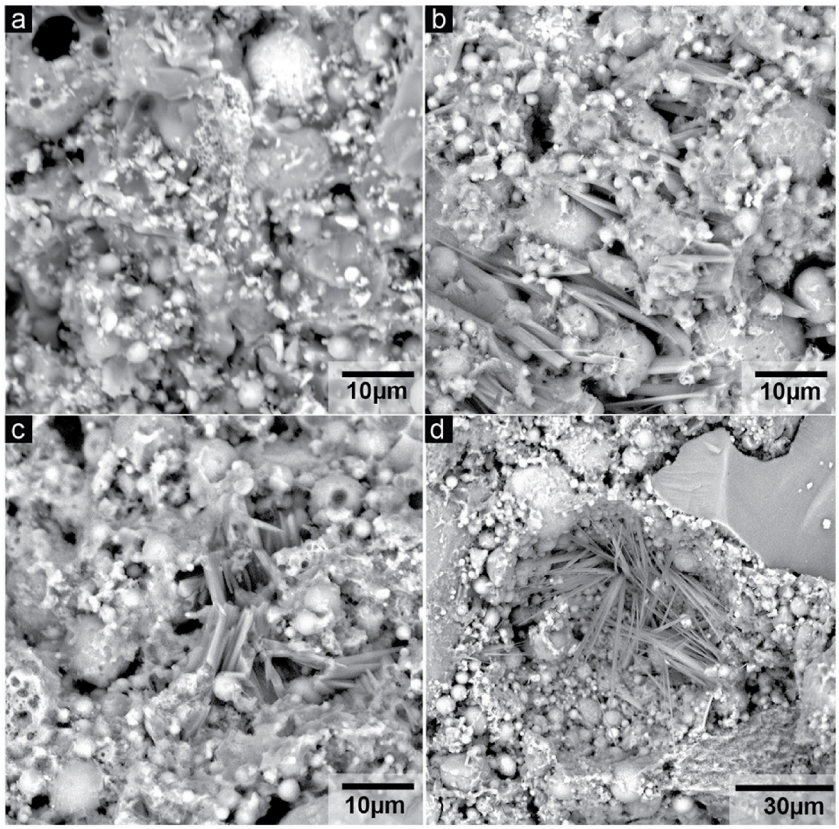

Fig. 25. SEM Images of HA and *Meta*-halloysite Geopolymer Mortars: (a) Control group; (b) HA-reinforced geopolymer; (c and d) *Meta*-halloysite-reinforced geopolymer [51].

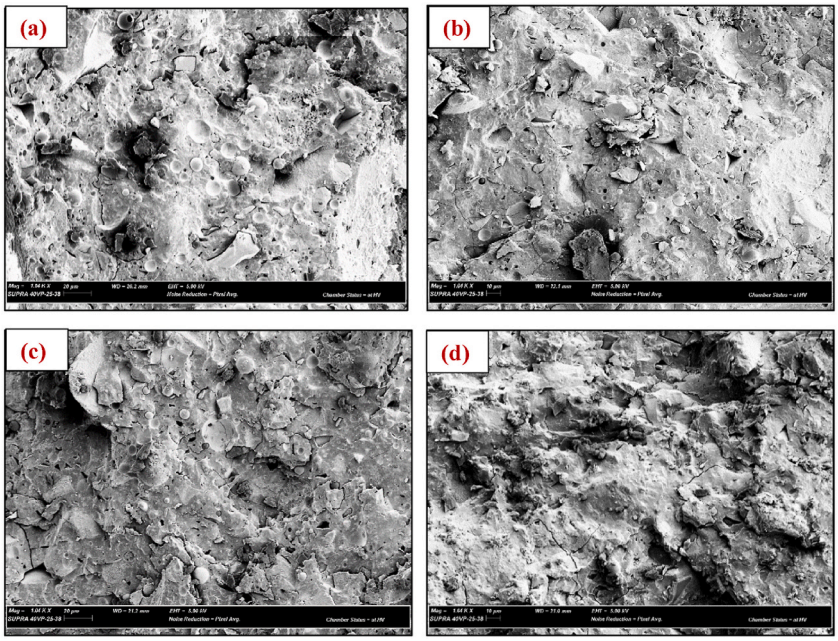

Fig. 26. Effect of introduced content of waste bricks on the microstructure of 3D printed fly ash-slag geopolymer: (a) 0 %; (b) 10 %; (c) 30 %; (d) 50 % [52].

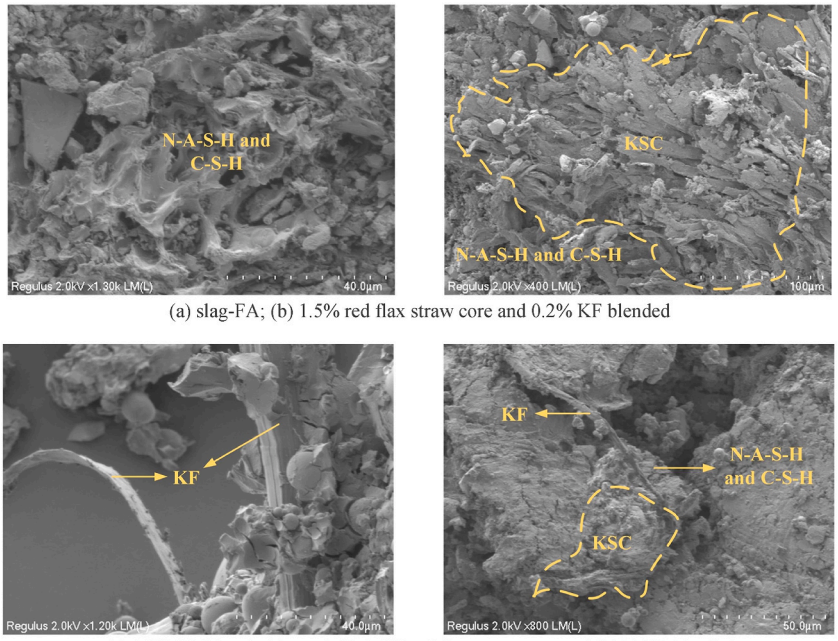

(a) slag-FA; (b) 1.5% red flax straw core and 0.2% KF blended

(c) 0.2% KF blended in; and (d) 1.5% red flax straw core and 0.2% KF blended

Fig. 27. Microscopic characteristics of fiber-reinforced 3D printed geopolymers [53].

were introduced, as shown in Fig. 27(c), the jute fibers exhibited internal bridging effects, contributing to enhanced crack resistance. When both KSC and KF were added to the geopolymer preparation, as shown in Fig. 27(d), the synergistic effect of KSC's framework and KF's bridging improved the microstructure of the geopolymer.

An appropriate amount of calcium-containing component in slag (CaO: 35–45 %) can effectively improve the microstructure. This is mainly due to the formation of calcium-rich gels in the system when mixed with slag. These gels provide more nucleation sites for the formation of geopolymer products, facilitating the better dissolution of silicon and aluminum components from the raw materials. As a result, the gelation process is accelerated, leading to an increased microstructural density of the geopolymer products.

Previous studies [124–126] have shown that the initial content of Si, Al, and Ca in silicon-aluminate raw materials had a significant

influence on the development of the geopolymer gel structure and microstructure. Al promoted the reaction rate of geopolymerisation, increasing the extent of reaction and product formation. Si contributed to the growth of geopolymer strength and improved its mechanical properties. Ca aided in the formation and stabilization of a three-dimensional network structure, further enhancing the strength and stability of geopolymer materials. Increasing the Si/Al ratio and Si/Ca ratio within a certain range could result in a more uniform and dense gel structure. This was because the molar ratio of Si and Al affected the connectivity and spatial arrangement of Si–O and Al–O bonds in the gel, thus influencing the gel's structure and stability. An appropriate molar ratio could effectively control the formation path and structure of the gel, leading to the desired microstructure.

According to previous studies [127–134], the relationship between different categories of gels and raw material components has been plotted, as shown in Fig. 28. The results indicate that (N, C)-A-S-H gel is more likely to form in systems rich in Al, while C-(A)-S-H gel tends to form in Si-rich systems. However, regardless of the changes in gel type, systems with high CaO and low Al content are unfavorable for the formation of gel products. On the other hand, in addition to reactive aluminosilicate minerals, new types of materials such as nanomaterials and fiber materials also play a role in modifying the microstructure, such as bridging and toughening. These findings were consistent with those reported by Garcia-Lodeiro et al. [135]. Therefore, these mentions above suggest that the composition of raw materials, including the Si, Al, and Ca content, as well as the inclusion of other materials, influences the formation of different types of gels and their impact on the microstructure of geopolymer materials.

6. Carbon footprint, environmental and economic benefits

Cost analysis and carbon footprint of 3D printing geopolymers are important. By analyzing the cost of 3D printing geopolymers, the economic feasibility of the process can be determined, the cost-effectiveness of different materials can be evaluated, and methods to reduce production costs can be identified. Additionally, studying the carbon footprint helps understand the environmental impact of 3D printing geopolymers. By assessing its carbon emissions and energy consumption, we can determine the potential of the process in terms of environmental sustainability. Reducing the carbon footprint is crucial for achieving the goals of reducing GHG emissions and addressing climate change.

Compared to conventional construction procedure, the 3D printing system has a lower environmental impact due to the elimination of scaffolding and formwork, which means that it also has a negligible cost and environmental impact on conventional construction. Fig. 29 depicts the energy consumption and carbon dioxide emissions linked with geopolymer and cement products in a 3D printing context. The majority of carbon emissions (95 %) and energy consumption (98 %) associated with 3D-printed geopolymers result from raw materials and alkaline activators. For OPC blends, OPC is the primary source of both CO_2 emissions and energy consumption. In contrast, low-carbon OPC blends entail utilizing alternative raw materials such as fly ash, slag or brick dust in the preparation of low-carbon cement. This results in a decrease in the demand for cement, leading to substantially lower energy consumption and carbon emissions compared to OPC blends. However, it is worth noting that 3D printed geopolymers frequently exhibit superior carbon emissions performance due to the usage of relatively low-carbon raw materials, whilst low-carbon cements aim to mitigate the environmental impact of traditional cements.

The construction and building materials industry has always been committed to achieving sustainable development and green structures, with the demand for using cheaper and widely available precursor materials and conducting whole life cycle design being the main driving force. However, in a dynamic and complex environment, these efforts are limited by the static perspective of material

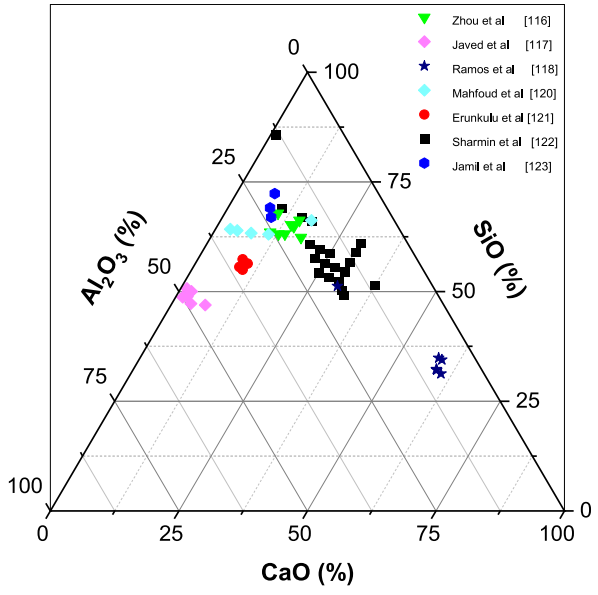

Fig. 28. Link between chemical composition of raw materials and gel products.

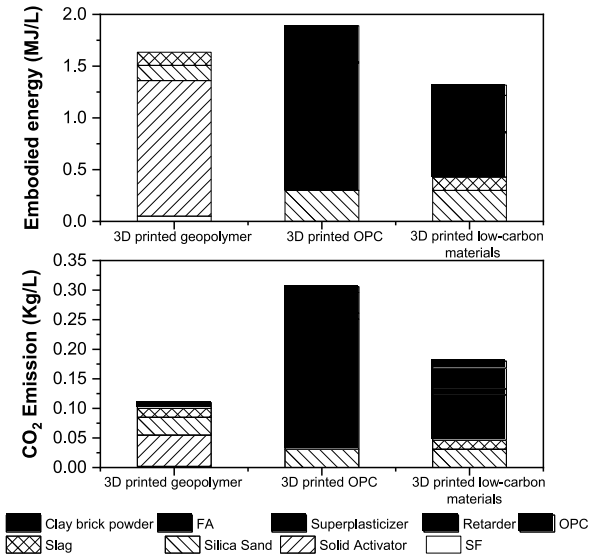

Fig. 29. Comparison of 3D printed geopolymers and cementitious materials in terms of environmental benefits: (a) CO_2 emissions; (b) energy consumption [54, 136,137].

supply. In such an environment, the introduction of new materials often means a shortage of another material. To overcome these limitations, it is essential to adopt a holistic approach that considers the interdependencies and cascading effects of material choices. This approach involves evaluating the environmental impact and resource availability of materials throughout their entire life cycle, from extraction or production to disposal or recycling. By understanding the life cycle implications of different materials, it becomes possible to make informed decisions that promote sustainability and minimize resource depletion [138–140].

Geopolymer production typically boasts low energy consumption and low emissions of pollutants. It can utilize a significant amount of waste materials as precursors, enhancing the sustainability of both the products and the manufacturing process while

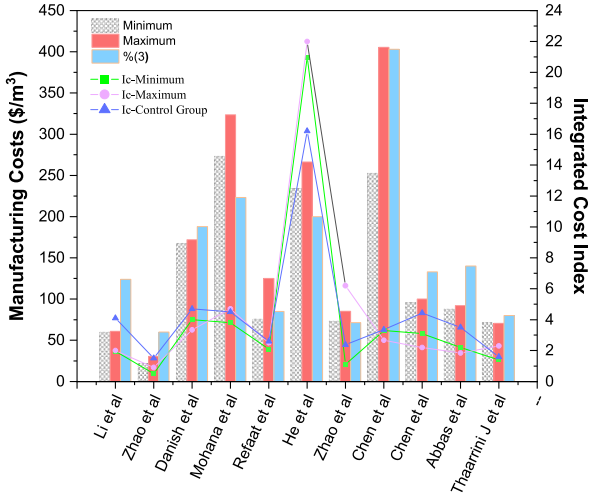

Chen et al [98]: * reactive ultra-fine fly ash-red mud-recycled powder
Thaarrini J et al [135]: * Bottom ash-Slag
Abbas et al [136]: * Egyptian kaolin clay
Chen et al [137]: * waste rubber-recycled steel
Zhao et al [138]: * one-part rubberized geopolymer
He et al [139]: * low concentration phosphoric acid-activated fly ash
Refaat et al [140]: *Slag
Mohana et al [141] : * nano fly ash
Danish et al [142]: * waste marble powder-Slag
Zhao et al [143]: * Sewage sludge ash-Slag
Li et al [144]: *Slag-fly ash

Fig. 30. The 3D printed geopolymer cost feasibility analysis.

adding new value throughout their lifecycle [141]. These waste materials or by-products are employed in the preparation of geopolymers, resulting in materials with diverse characteristics. Rice husk (RH), FA, GGBS, agricultural by-products, and kaolin clay are commonly used as major precursors [142–146]. Some of these major precursors, including waste and low-cost enriched materials that are widely used in the production of geopolymer materials, are briefly described below.

To assess the economic efficiency of the geopolymers under study, the composite cost index, I_c ($/m^3/MPa), was calculated by Eq. (1).

$$I_c = C_t / f_{c28} \tag{1}$$

where I_c represents the comprehensive cost index, C_t ($/m^3) is the cost of geopolymer per cubic meter, and f_{c28} (MPa) represents the 28-day compressive strength of the geopolymer. The magnitude of the geopolymer comprehensive cost index is significant. A smaller comprehensive cost index indicates a relatively lower overall cost of using geopolymer materials. This suggests that using such materials may have economic advantages and potentially result in lower cost burdens [147]. Additionally, a smaller comprehensive cost index also indicates advantages in sustainability, including lower maintenance costs, a lower carbon footprint, and better mechanical performance.

We have analysed the previous studies with a comprehensive cost index [110,148–157], as shown in Fig. 30, and it seems that most of the prepared geopolymers cost less than the control group (traditional building materials such as cement, concrete, etc.), however, there are still a number of studies in which the cost of the prepared geopolymers is close to or far more than that of the traditional building materials.

Li et al. [157] pointed out that compared to ordinary concrete, alkali-activated slag-FA geopolymer concrete could reduce production costs and carbon emissions by 15.7 % and 73.8 %, respectively. Zhao et al. [156] found that the I_c of single component geopolymer was about 15 % higher than that of binary geopolymer. To achieve the desired mechanical performance, single component geopolymer required a higher dosage of alkali activators, which increased its cost. Mohana et al. [154] demonstrated that geopolymer mortars obtained from pre-treated FA did not require any superplasticizers (SP), resulting in cost savings. However, when developing geopolymer mortar with nano-fillers, the cost was 19 % higher than cement mortar, mainly due to the expensive nanomaterials used. He et al. [152] also pointed out that although FA-based geopolymer was considered a more sustainable material with significantly lower CO_2 emissions, energy consumption, and cost compared to cement, this study used the environmentally friendly material phosphoric acid (which has higher carbon emissions and energy) at a higher cost, leading to a substantial increase in production costs.

Therefore, while developing geopolymers using different solid wastes such as FA, slag, and waste construction material powder presents a potentially economically viable approach with relatively low costs, the evaluation of the prices and supply stability of different alkali activators, as well as the activation potential of selected raw materials, is still necessary to find affordable and quality-stable alkali activators. Compared to other traditional building materials, there is currently a relative lack of research on the cost aspects of geopolymer production.

On the other hand, based on previous studies [158], we draw the carbon footprints of different materials to easily analyse whether they have potential environmental value, as shown in Fig. 31. Overall, using materials that require a significant amount of energy tends to result in higher carbon footprints. This is because the production and manufacturing processes of these materials consume a large amount of energy and often rely on fossil fuels. For example, materials such as rubber, PVC pipes, and fibers require high-temperature treatment, chemical processes, or mechanical processing during their preparation and processing, which typically involve substantial energy usage. In contrast, industrial by-products such as FA and slag are by-products of industrial processes, and they can be reused as

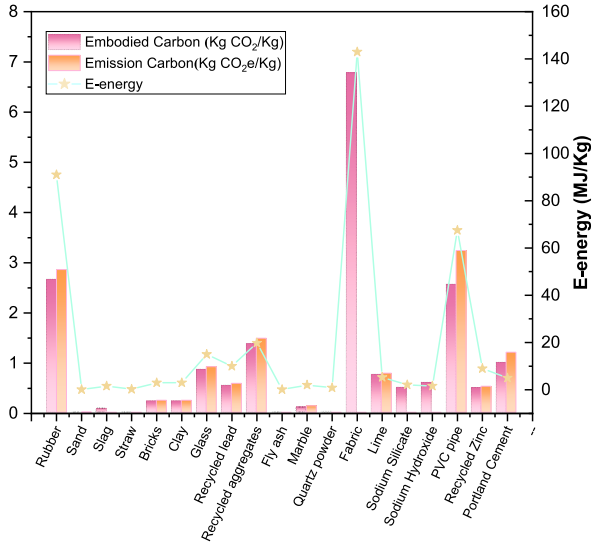

Fig. 31. Carbon footprint and energy consumption of different raw materials.

part of materials. The production process of these by-products consumes relatively less energy because they are derived from other industrial processes. Natural sand and stone can also be obtained through simple mining processes, which have relatively low energy consumption. Recycled aggregates are materials obtained from reclaimed and reused waste concrete and construction materials, and the energy consumed in their production process is also relatively low. Additionally, there are emerging materials that do not require high-temperature heating or processing but more energy-consumption. For example, the preparation of nanomaterials typically requires high energy input. In general, choosing materials with lower energy consumption, particularly industrial by-products and natural materials, can reduce the carbon footprint of construction and manufacturing processes and contribute to sustainable development.

Geopolymer products typically have lower energy demand and carbon emissions compared to traditional OPC-related products. When it comes to building materials, calculating energy demand mainly involves the energy consumption for producing cement clinker, sand, gypsum, and coarse aggregates [159,160]. The preparation process of OPC usually involves high-temperature calcination of limestone and clay, which requires a significant amount of energy and generates a large amount of carbon dioxide emissions.

On the other hand, in the preparation process of geopolymer products, the main energy demand comes from the production of raw materials. Common raw materials for geopolymers, such as FA and GGBS, are usually byproducts of industrial processes. They do not require high-temperature treatment, resulting in relatively lower energy consumption. Furthermore, the production process of commonly used alkaline activators like sodium silicate and sodium hydroxide also typically requires much less energy compared to the production of cement [161]. Furthermore, some researchers claim that the production of geopolymer products can have zero energy demand [162]. Some of them point out that to achieve better energy performance, it is preferable to consider the energy required for collecting, grinding, and processing all the raw materials [163,164].

7. Conclusions

The 3D printing of geopolymer systems, the effect of raw materials on processability (e.g., including flowability and thixotropy), and microstructure are comprehensively reviewed in this paper. The conclusions drawn are as follows.

(1) By introducing the raw materials and alkaline activator through separate feed pipes into the hopper of the 3D printing system, it is possible to effectively avoid the inconveniences caused by initial mixing, such as the formation of clumps and overly viscous slurry.
(2) The molding zone near the nozzle outlet is subject to two types of resistance: slurry pressure and wall friction, with wall friction being an important factor affecting the extrusion resistance of the fluid as it passes through the nozzle of the 3D printing system. The strength of these resistance forces is determined by the cone angle of the conical region.
(3) Nozzle design needs to be considered when it comes to 3D printing geopolymers as it affects factors such as print quality, accuracy, and flow. It has been shown that square nozzles provide better surface smoothness than oval nozzles. In addition, nozzle design should aim to reduce extrusion resistance to achieve good print quality.
(4) The solid proportion of inert materials and the chemical composition of the raw materials significantly affect the setting time of 3D printed geopolymer materials. From a physical perspective, increasing the solid ratio of inert materials can shorten the setting time, and materials with high water absorption can accelerate the reaction process. On the chemical level, the geopolymerisation degree of the silicate solution plays a crucial role in the gelation of the slurry: the higher the geopolymerisation degree, the smaller the volume of colloidal particles and the stronger the reaction activity.
(5) Geopolymer is a suspension of liquid and solid dispersants, and its rheological properties are influenced by colloidal and inertial contact between particles, particle solubility, and the viscous interaction with alkaline agents. The elemental composition of the precursor of the aluminosilicate also plays a crucial role in controlling the rheological behaviour of geopolymer.
(6) Raw materials with high soluble reactive silica, increasing the SiO_2/Al_2O_3 ratio of the raw material, and increasing the CaO content of the matrix help to improve the compressive strength of 3D printed geopolymers. The dissolution of Si and Al in silicoaluminate materials is closely related to the alkaline activator, and the dissolution of Si and Al directly affects the formation of geopolymer products.
(7) The main factors that influence the interlayer strength of 3D printed geopolymer can be divided into chemical and physical factors, which are affected by the raw materials used. In terms of chemical factors, the reactivity of the raw materials is an important factor affecting interlayer bonding. Raw materials with high reactivity can have both positive and negative effects. On one hand, they can reduce interlayer porosity and improve the interface transition zone. On the other hand, these materials can also lead to areas of poor drying and inadequate bonding. Regarding physical factors, the interfacial humidity field and moisture transfer are key factors that affect the mechanical properties of the interface. Proper moisture distribution and transfer are crucial for achieving strong interlayer bonding and ensuring the overall structural integrity of the printed geopolymer.
(8) The initial content of silicon, aluminum, and calcium in the raw materials of aluminosilicates has an important influence on the development of the gel structure and microstructure of geopolymer. Al promotes the reaction rate of geopolymerisation, increasing the extent of reaction and product formation. Si helps improve the strength of geopolymer and enhances its mechanical properties. Ca contributes to the formation and stability of the three-dimensional network structure, further improving the strength and stability of geopolymer materials.
(9) The majority of carbon emissions, energy consumption, and cost associated with 3D printed geopolymer come from the raw materials and alkaline activators. Therefore, geopolymer is considered a more sustainable material compared to cement, as it

significantly reduces carbon dioxide emissions, energy consumption, and costs. However, it is important to note that the production costs of alkaline activators need to be considered when using geopolymer.

In conventional manufacturing of geopolymer materials, certain source materials (usually industrial by-products or naturally occurring minerals high in alumina and silica) are primarily amalgamated with alkaline activators to harden into a sustainable structure. Conversely, fabricating geopolymer materials through 3D printing utilizing a step-by-step deposition tactic offers fresh prospects and difficulties. Raw materials have a crucial impact on the rheological behaviour, interlayer bonding, microstructure, and mechanical properties of printed samples. To achieve successful geopolymer 3D printing, it is essential to fine-tune the composition of raw materials. This involves adjusting the solid ratio of inert materials, the chemical composition of raw materials, the elemental composition of aluminosilicate precursors, and increasing the silica-aluminium ratio in raw materials. Additionally, when selecting raw materials with high reactivity (including those containing highly soluble reactive silica) and alkaline activators, the printability, layer adhesion, mechanical properties, and structural integrity of 3D printed geopolymer structures may also be affected.

8. Suggestions

Based on the review in this article, some suggestions can be used for reference as follows.

(1) To further investigate the optimal composition of geopolymer raw materials (silicate sources containing silicon, aluminium and calcium) for 3D printing applications. Printing applications, by exploring different ratios or combinations of these elements to improve the gel structure, microstructure development and mechanical properties of geopolymer-based materials.
(2) Extensive research into the microstructure of 3D printed geopolymer materials should also be undertaken, where various imaging and analytical methods will establish links between raw material composition, gel structure and mechanical properties at the microscopic level.
(3) Methods to enhance the reactivity of synthetic feedstocks for geopolymers should be evaluated. To examine additives or treatments that augment the reactivity of silicon, aluminium and calcium sources, potentially enhancing interlayer bonding and mechanical properties in 3D printed geopolymer structures.
(4) Future studies should focus on conducting a thorough life cycle evaluation comparing 3D-printed geopolymer materials to conventional cement-based materials, and the assessment should not only investigate the direct carbon emissions and energy usage, but also consider the environmental effect of the substances during their entire life cycle, including manufacturing, usage, and disposal.
(5) Exploring methods to optimize the 3D printing process of geopolymer materials for the purpose of reducing carbon emissions, energy consumption, and costs is really crucial.

CRediT authorship contribution statement

Kailun Chen: Data curation, Formal analysis, Investigation, Methodology, Writing – original draft, Writing – review & editing. **Qiong Liu:** Writing – original draft, Writing – review & editing. **Bing Chen:** Writing – original draft, Writing – review & editing. **Shishun Zhang:** Writing – original draft, Writing – review & editing. **Liberato Ferrara:** Writing – original draft, Writing – review & editing. **Wengui Li:** Conceptualization, Funding acquisition, Methodology, Resources, Supervision, Writing – original draft, Writing – review & editing.

Declaration of competing interest

The authors declare that they have no known competing financial interests or personal relationships that could have appeared to influence the work reported in this paper.

Data availability

Data will be made available on request.

Acknowledgment

The authors appreciate the support from Australian Research Council (ARC), Australia (FT220100177, LP230100288, DP220100036, DP220101051, IH200100010).

References

[1] B. Rangel, A.S. Guimarães, J. Lino, L. Santana, 3D Printing for Construction with Alternative Materials, Springer Cham, 2023, https://doi.org/10.1007/978-3-031-09319-7.
[2] H. Tu, Z. Wei, A. Bahrami, N. Ben Kahla, A. Ahmad, Y.O. Özkılıç, Recent Advancements and Future Trends in 3D Printing Concrete Using Waste Materials, Developments in the Built Environment, 2023 100187, https://doi.org/10.1016/J.DIBE.2023.100187.
[3] Y. Wang, L. chao Qiu, Y. ye Hu, S. gui Chen, Y. Liu, Influential factors on mechanical properties and microscopic characteristics of underwater 3D printing concrete, J. Build. Eng. 77 (2023), https://doi.org/10.1016/j.jobe.2023.107571.
[4] P. Duan, C. Yan, W. Zhou, D. Ren, Development of fly ash and iron ore tailing based porous geopolymer for removal of Cu(II) from wastewater, Ceram. Int. 42 (2016) 13507–13518, https://doi.org/10.1016/J.CERAMINT.2016.05.143.

[5] Y. Ettahiri, B. Bouargane, K. Fritah, B. Akhsassi, L. Pérez-Villarejo, A. Aziz, L. Bouna, A. Benlhachemi, R.M. Novais, A state-of-the-art review of recent advances in porous geopolymer: applications in adsorption of inorganic and organic contaminants in water, Construct. Build. Mater. 395 (2023) 132269, https://doi.org/10.1016/J.CONBUILDMAT.2023.132269.

[6] C. Vlachakis, X. Wang, A. Al-Tabbaa, Investigation of the compressive self-sensing response of filler-free metakaolin geopolymer binders and coatings, Construct. Build. Mater. 392 (2023) 131682, https://doi.org/10.1016/J.CONBUILDMAT.2023.131682.

[7] S. Candamano, A. Policicchio, G. Conte, R. Abarca, C. Algieri, S. Chakraborty, S. Curcio, V. Calabrò, F. Crea, R.G. Agostino, Preparation of foamed and unfoamed geopolymer/NaX zeolite/activated carbon composites for CO2 adsorption, J. Clean. Prod. 330 (2022) 129843, https://doi.org/10.1016/J.JCLEPRO.2021.129843.

[8] J. Wang, Y. Luan, T. Ma, W. Zhang, G. Xu, Experimental investigation on the mechanical performance and microscopic characterization of desulfurization gypsum-reinforced ternary geopolymer, Construct. Build. Mater. 392 (2023) 131855, https://doi.org/10.1016/J.CONBUILDMAT.2023.131855.

[9] B. Ma, Z. Zhu, W. Huo, L. Yang, Y. Zhang, H. Sun, X. Zhang, Assessing the viability of a high performance one-part geopolymer made from fly ash and GGBS at ambient temperature, J. Build. Eng. 75 (2023) 106978, https://doi.org/10.1016/J.JOBE.2023.106978.

[10] A. Anburuvel, N. Sathiparan, G.M.A. Dhananjaya, A. Anuruththan, Characteristic evaluation of geopolymer based lateritic soil stabilization enriched with eggshell ash and rice husk ash for road construction: an experimental investigation, Construct. Build. Mater. 387 (2023) 131659, https://doi.org/10.1016/J.CONBUILDMAT.2023.131659.

[11] Y.P. Luo, Y. Lv, D. Wang, Z. Jiang, G. Xue, The influence of coarse aggregate gradation on the mechanical properties, durability, and plantability of geopolymer pervious concrete, Construct. Build. Mater. 382 (2023) 131246, https://doi.org/10.1016/J.CONBUILDMAT.2023.131246.

[12] J. Upadhyay, S.P. Misra, S. Irusta, S. Sharma, P.A. Deshpande, Oxidation of aldehydes to carboxylic acids over geopolymer supported CuO, Mol. Catal. 536 (2023) 112911, https://doi.org/10.1016/J.MCAT.2022.112911.

[13] H. Yang, F. Dai, H. Chen, Y. He, Z. Wang, R. Wang, Fabrication of stalk fiber/geopolymers-based slow-release fertilizer with agricultural waste and loess for promoting plant growth, J. Environ. Chem. Eng. 11 (2023) 109481, https://doi.org/10.1016/J.JECE.2023.109481.

[14] Major Countries in Worldwide Cement Production in 2022, Statista, 2023. https://www.statista.com/statistics/267364/world-cement-production-by-country/. (Accessed 10 December 2023).

[15] Production Volume of Cement Worldwide from 1995 to 2022, Statista, 2023. https://www.statista.com/statistics/1087115/global-cement-production-volume/. (Accessed 10 December 2023).

[16] Global Cement Outlook, On Field Investment Research, 2019. https://ics-canada.ca/wp-content/uploads/2019/12/On-Field-Research-Global-Cement-Outlook-Summary-for-attendees.pdf. (Accessed 10 December 2023).

[17] R. Chaudhury Supriya, U. Sharma, P.C. Thapliyal, L.P. Singh, Low-CO2 emission strategies to achieve net zero target in cement sector, J. Clean. Prod. 417 (2023) 137466, https://doi.org/10.1016/J.JCLEPRO.2023.137466.

[18] Carbon Dioxide Emissions from the Manufacture of Cement Worldwide in from 1990 to 2022, Statista, 2023. https://www.statista.com/statistics/1091672/carbon-dioxide-emissions-global-cement-manufacturing/. (Accessed 10 December 2023).

[19] W. Li, Z. Luo, Y. Gan, K. Wang, S.P. Shah, Nanoscratch on mechanical properties of interfacial transition zones (ITZs) in fly ash-based geopolymer composites, Compos. Sci. Technol. 214 (2021) 109001.

[20] J. Fan, J. Yan, M. Zhou, Y. Xu, Y. Lu, P. Duan, Y. Zhu, Z. Zhang, W. Li, A. Wang, D. Sun, Heavy metals immobilization of ternary geopolymer based on nickel slag, lithium slag and metakaolin, J. Hazard. Mater. 453 (2023) 131380.

[21] Z. Tang, W. Li, Q. Peng, L. Yan, Quasi-static cyclic behavior of CFRP-confined geopolymeric composites, J. Compos. Constr. 27 (6) (2023) 04023051.

[22] Y. Li, H. Zhao, Y. Hu, F. Qu, D. Zhu, K. Wang, W. Li, Effect of pore water pressure on mechanical performance of recycled aggregate concrete under triaxial compression, Cem. Concr. Compos. 146 (2024) 105402.

[23] J. Zhang, J. Wang, S. Dong, X. Yu, B. Han, A review of the current progress and application of 3D printed concrete, Composer Part A Appl Sci Manuf 125 (2019) 105533, https://doi.org/10.1016/J.COMPOSITESA.2019.105533.

[24] J. Xiao, S. Zou, Y. Yu, Y. Wang, T. Ding, Y. Zhu, J. Yu, S. Li, Z. Duan, Y. Wu, L. Li, 3D recycled mortar printing: system development, process design, material properties and on-site printing, J. Build. Eng. 32 (2020) 101779, https://doi.org/10.1016/J.JOBE.2020.101779.

[25] E. Ivan Diaz-Loya, Erez N. Allouche, Saiprasad Vaidya, Mechanical properties of fly-ash-based geopolymer concrete, ACI Mater. J. 108 (2011) 300.

[26] A. Kashani, J.L. Provis, G.G. Qiao, J.S.J. Van Deventer, The interrelationship between surface chemistry and rheology in alkali activated slag paste, Construct. Build. Mater. 65 (2014) 583–591, https://doi.org/10.1016/J.CONBUILDMAT.2014.04.127.

[27] S. Muthukrishnan, S. Ramakrishnan, J. Sanjayan, Set on demand geopolymer using print head mixing for 3D concrete printing, Cem. Concr. Compos. 128 (2022) 104451, https://doi.org/10.1016/J.CEMCONCOMP.2022.104451.

[28] S. Yu, J. Sanjayan, H. Du, Effects of cement mortar characteristics on aggregate-bed 3D concrete printing, Addit. Manuf. 58 (2022) 103024, https://doi.org/10.1016/J.ADDMA.2022.103024.

[29] I. Mai, D. Lowke, A. Perrot, Fluid intrusion in powder beds for selective cement activation – an experimental and analytical study, Cement Concr. Res. 156 (2022) 106771, https://doi.org/10.1016/J.CEMCONRES.2022.106771.

[30] Q. Lyu, P. Dai, A. Chen, Sandwich-structured porous concrete manufactured by mortar-extrusion and aggregate-bed 3D printing, Construct. Build. Mater. 392 (2023) 131909, https://doi.org/10.1016/J.CONBUILDMAT.2023.131909.

[31] S. Yu, J. Sanjayan, H. Du, Impact of particle size and grading on aggregate-bed 3D concrete printing, in: F.P. Bos, S.S. Lucas, R.J.M. Wolfs, T.A.M. Salet (Eds.), Second RILEM International Conference on Concrete and Digital Fabrication, Springer International Publishing, Cham, 2020, pp. 557–563.

[32] S. Yu, H. Du, J. Sanjayan, Aggregate-bed 3D concrete printing with cement paste binder, Cement Concr. Res. 136 (2020) 106169, https://doi.org/10.1016/J.CEMCONRES.2020.106169.

[33] N. Zhang, J. Sanjayan, Extrusion nozzle design and print parameter selections for 3D concrete printing, Cem. Concr. Compos. 137 (2023) 104939, https://doi.org/10.1016/J.CEMCONCOMP.2023.104939.

[34] H. Khelifi, A. Perrot, T. Lecompte, D. Rangeard, G. Ausias, Prediction of extrusion load and liquid phase filtration during ram extrusion of high solid volume fraction pastes, Powder Technol. 249 (2013) 258–268, https://doi.org/10.1016/J.POWTEC.2013.08.023.

[35] A.H. Behravesh, E. Shakouri, A. Zolfaghari, M. Golzar, Theoretical and experimental study on die pressure prediction in extrusion of wood-plastic composite, J. Compos. Mater. 44 (2010) 1293–1304, https://doi.org/10.1177/0021998309352703.

[36] S. Chaves Figueiredo, C. Romero Rodríguez, Z.Y. Ahmed, D.H. Bos, Y. Xu, T.M. Salet, O. Çopuroğlu, E. Schlangen, F.P. Bos, An approach to develop printable strain hardening cementitious composites, Mater. Des. 169 (2019) 107651, https://doi.org/10.1016/J.MATDES.2019.107651.

[37] A. Perrot, Y. Mélinge, D. Rangeard, F. Micaelli, P. Estellé, C. Lanos, Use of ram extruder as a combined rheo-tribometer to study the behaviour of high yield stress fluids at low strain rate, Rheol. Acta 51 (2012) 743–754, https://doi.org/10.1007/s00397-012-0638-6.

[38] M. Chougan, S. Hamidreza Ghaffar, M. Jahanzat, A. Albar, N. Mujaddedi, R. Swash, The influence of nano-additives in strengthening mechanical performance of 3D printed multi-binder geopolymer composites, Construct. Build. Mater. 250 (2020) 118928, https://doi.org/10.1016/J.CONBUILDMAT.2020.118928.

[39] C. Sun, J. Xiang, M. Xu, Y. He, Z. Tong, X. Cui, 3D extrusion free forming of geopolymer composites: materials modification and processing optimization, J. Clean. Prod. 258 (2020) 120986, https://doi.org/10.1016/J.JCLEPRO.2020.120986.

[40] N. Ranjbar, M. Mehrali, C. Kuenzel, C. Gundlach, D.B. Pedersen, A. Dolatshahi-Pirouz, J. Spangenberg, Rheological characterization of 3D printable geopolymers, Cement Concr. Res. 147 (2021) 106498, https://doi.org/10.1016/J.CEMCONRES.2021.106498.

[41] S. Muthukrishnan, S. Ramakrishnan, J. Sanjayan, Effect of alkali reactions on the rheology of one-part 3D printable geopolymer concrete, Cem. Concr. Compos. 116 (2021) 103899, https://doi.org/10.1016/J.CEMCONCOMP.2020.103899.

[42] G. Ma, Y. Yan, M. Zhang, J. Sanjayan, Effect of steel slag on 3D concrete printing of geopolymer with quaternary binders, Ceram. Int. 48 (2022) 26233–26247, https://doi.org/10.1016/J.CERAMINT.2022.05.305.

[43] A.V. Rahul, M. Santhanam, H. Meena, Z. Ghani, 3D printable concrete: mixture design and test methods, Cem. Concr. Compos. 97 (2019) 13–23, https://doi.org/10.1016/J.CEMCONCOMP.2018.12.014.

[44] S.C. Paul, Y.W.D. Tay, B. Panda, M.J. Tan, Fresh and hardened properties of 3D printable cementitious materials for building and construction, Arch. Civ. Mech. Eng. 18 (2018) 311–319, https://doi.org/10.1016/J.ACME.2017.02.008.

[45] A. Kazemian, X. Yuan, E. Cochran, B. Khoshnevis, Cementitious materials for construction-scale 3D printing: laboratory testing of fresh printing mixture, Construct. Build. Mater. 145 (2017) 639–647, https://doi.org/10.1016/J.CONBUILDMAT.2017.04.015.

[46] P. Nasruldeen Shakor, Investigation of Cementitious Materials and Fibre Reinforced Mortar in 3D Printing, Doctoral Thesis, University of Technology Sydney, 2019.

[47] S.C. Paul, G.P.A.G. van Zijl, I. Gibson, A review of 3D concrete printing systems and materials properties: current status and future research prospects, Rapid Prototyp. J. 24 (2018) 784–798, https://doi.org/10.1108/RPJ-09-2016-0154.

[48] L.H. Anell, Concrete 3d Printer, Master Thesis, Lund University, 2015.

[49] A. Hadian, B. Morath, M. Biedermann, M. Meboldt, F. Clemens, Selected design rules for material extrusion-based additive manufacturing of alumina based nozzles and heat exchangers considering limitations in printing, debinding, and sintering, Addit. Manuf. 75 (2023) 103719, https://doi.org/10.1016/J.ADDMA.2023.103719.

[50] F. Salari, P. Bosetti, V.M. Sglavo, Binder jetting 3D printing of magnesium oxychloride cement-based materials: parametric analysis of manufacturing factors, Journal of Manufacturing and Materials Processing 6 (2022), https://doi.org/10.3390/jmmp6040086.

[51] N. Ranjbar, C. Kuenzel, C. Gundlach, P. Kempen, M. Mehrali, Halloysite reinforced 3D-printable geopolymers, Cem. Concr. Compos. 136 (2023) 104894, https://doi.org/10.1016/J.CEMCONCOMP.2022.104894.

[52] K. Pasupathy, S. Ramakrishnan, J. Sanjayan, 3D concrete printing of eco-friendly geopolymer containing brick waste, Cem. Concr. Compos. 138 (2023) 104943, https://doi.org/10.1016/J.CEMCONCOMP.2023.104943.

[53] X. Kong, L. Dai, Y. Wang, D. Qiao, S. Hou, S. Wang, Influence of kenaf stalk on printability and performance of 3D printed industrial tailings based geopolymer, Construct. Build. Mater. 315 (2022) 125787, https://doi.org/10.1016/J.CONBUILDMAT.2021.125787.

[54] S.H. Bong, M. Xia, B. Nematollahi, C. Shi, Ambient temperature cured 'just-add-water' geopolymer for 3D concrete printing applications, Cem. Concr. Compos. 121 (2021) 104060, https://doi.org/10.1016/J.CEMCONCOMP.2021.104060.

[55] P.N. Lemougna, A. Nzeukou, B. Aziwo, A.B. Tchamba, K. tuo Wang, U.C. Melo, X. min Cui, Effect of slag on the improvement of setting time and compressive strength of low reactive volcanic ash geopolymers synthetized at room temperature, Mater. Chem. Phys. 239 (2020) 122077, https://doi.org/10.1016/J.MATCHEMPHYS.2019.122077.

[56] C.R. Kaze, G.L. Lecomte-Nana, A. Adesina, J.G.D. Nemaleu, E. Kamseu, U. Chinje Melo, Influence of mineralogy and activator type on the rheology behaviour and setting time of laterite based geopolymer paste, Cem. Concr. Compos. 126 (2022), https://doi.org/10.1016/j.cemconcomp.2021.104345.

[57] C. Dupuy, J. Havette, A. Gharzouni, N. Texier-Mandoki, X. Bourbon, S. Rossignol, Metakaolin-based geopolymer: formation of new phases influencing the setting time with the use of additives, Construct. Build. Mater. 200 (2019) 272–281, https://doi.org/10.1016/j.conbuildmat.2018.12.114.

[58] X. Ma, Y. Zhao, M. Liu, Y. Xia, Y. Yang, Sodium gluconate as a retarder modified sewage sludge ash-based geopolymers: mechanism and environmental assessment, J. Clean. Prod. 419 (2023) 138317, https://doi.org/10.1016/j.jclepro.2023.138317.

[59] A. Hoayek, M. Khalifeh, H. Hamie, B. El-Ghoul, R. Zogheib, Prediction of geopolymer pumpability and setting time for well zonal isolation - using machine learning and statistical based models, Heliyon 9 (2023), https://doi.org/10.1016/j.heliyon.2023.e17925.

[60] M.N.S. Hadi, H. Zhang, S. Parkinson, Optimum mix design of geopolymer pastes and concretes cured in ambient condition based on compressive strength, setting time and workability, J. Build. Eng. 23 (2019) 301–313, https://doi.org/10.1016/j.jobe.2019.02.006.

[61] A.A. Siyal, K.A. Azizli, Z. Man, H. Ullah, Effects of parameters on the setting time of fly ash based geopolymers using taguchi method, in: Procedia Eng, Elsevier Ltd, 2016, pp. 302–307, https://doi.org/10.1016/j.proeng.2016.06.624.

[62] M. Arnoult, M. Perronnet, A. Autef, S. Rossignol, How to control the geopolymer setting time with the alkaline silicate solution, J. Non-Cryst. Solids 495 (2018) 59–66, https://doi.org/10.1016/j.jnoncrysol.2018.02.036.

[63] N. Nikoloutsopoulos, A. Sotiropoulou, G. Kakali, S. Tsivilis, The Effect of Solid/Liquid Ratio on Setting Time, Workability and Compressive Strength of Fly Ash Based Geopolymers, 2018, in: www.sciencedirect.comwww.materialstoday.com/proceedings2214-7853.

[64] B. Panda, C. Unluer, M.J. Tan, Extrusion and rheology characterization of geopolymer nanocomposites used in 3D printing, Compos. B Eng. 176 (2019) 107290, https://doi.org/10.1016/J.COMPOSITESB.2019.107290.

[65] X. Guo, J. Yang, G. Xiong, Influence of supplementary cementitious materials on rheological properties of 3D printed fly ash based geopolymer, Cem. Concr. Compos. 114 (2020) 103820, https://doi.org/10.1016/J.CEMCONCOMP.2020.103820.

[66] M. Chen, B. Liu, L. Li, L. Cao, Y. Huang, S. Wang, P. Zhao, L. Lu, X. Cheng, Rheological parameters, thixotropy and creep of 3D-printed calcium sulfoaluminate cement composites modified by bentonite, Compos. B Eng. 186 (2020) 107821, https://doi.org/10.1016/J.COMPOSITESB.2020.107821.

[67] L. Zhou, M. Gou, H. Zhang, Investigation on the applicability of bauxite tailings as fine aggregate to prepare 3D printing mortar, Construct. Build. Mater. 364 (2023) 129904, https://doi.org/10.1016/J.CONBUILDMAT.2022.129904.

[68] G.A. Ramos, P.R. de Matos, F. Pelisser, P.J.P. Gleize, Effect of porcelain tile polishing residue on eco-efficient geopolymer: rheological performance of pastes and mortars, J. Build. Eng. 32 (2020), https://doi.org/10.1016/j.jobe.2020.101699.

[69] H. Ilcan, O. Sahin, A. Kul, E. Ozcelikci, M. Sahmaran, Rheological property and extrudability performance assessment of construction and demolition waste-based geopolymer mortars with varied testing protocols, Cem. Concr. Compos. 136 (2023), https://doi.org/10.1016/j.cemconcomp.2022.104891.

[70] Y. Tian, Z. Xie, Q. Yuan, G.M. Jamaa, C. Yang, X. Zhu, Improving the rheological behavior of alkali-activated slag pastes by using low surface free energy mineral admixtures, Construct. Build. Mater. 392 (2023), https://doi.org/10.1016/j.conbuildmat.2023.131879.

[71] J. de Gasperi, D. Holthusen, M.F.D. Howes, N. Sattler, M.A. Longhi, E.D. Rodríguez, Temporal dynamics of rheological properties of metakaolin-based geopolymers: effects of synthesis parameters, Construct. Build. Mater. 289 (2021), https://doi.org/10.1016/j.conbuildmat.2021.123145.

[72] G. Gu, F. Xu, X. Huang, S. Ruan, C. Peng, J. Lin, Foamed geopolymer, The relationship between rheological properties of geopolymer paste and pore-formation mechanism, J. Clean. Prod. 277 (2020), https://doi.org/10.1016/j.jclepro.2020.123238.

[73] O. Mahmoodi, H. Siad, M. Lachemi, S. Dadsetan, M. Şahmaran, Extensive rheological evaluation of geopolymer mortars incorporating maximum amounts of recycled concrete as precursors and aggregates, Construct. Build. Mater. 390 (2023), https://doi.org/10.1016/j.conbuildmat.2023.131801.

[74] Q. Zhong, H. Nie, G. Xie, H. Peng, Experimental study on the characteristics, rheological factors, and flowability of MK-GGBFS geopolymer slurry, J. Build. Eng. 76 (2023), https://doi.org/10.1016/j.jobe.2023.107300.

[75] O. Mahmoodi, H. Siad, M. Lachemi, M. Şahmaran, Effects of mono and binary recycled aggregates on the rheological properties of geopolymer mortars synthesized with construction and demolition waste-based binders, J. Build. Eng. 77 (2023) 107545, https://doi.org/10.1016/j.jobe.2023.107545.

[76] C. Rodrigue Kaze, A. Adesina, T. Alomayri, H. Assaedi, E. Kamseu, U. Chinje Melo, C. Leonelli, Characterization, reactivity and rheological behaviour of metakaolin and Meta-halloysite based geopolymer binders, Cleaner Materials 2 (2021), https://doi.org/10.1016/j.clema.2021.100025.

[77] B. Panda, S.C. Paul, N.A.N. Mohamed, Y.W.D. Tay, M.J. Tan, Measurement of tensile bond strength of 3D printed geopolymer mortar, Measurement 113 (2018) 108–116, https://doi.org/10.1016/J.MEASUREMENT.2017.08.051.

[78] B. Panda, C. Unluer, M.J. Tan, Investigation of the rheology and strength of geopolymer mixtures for extrusion-based 3D printing, Cem. Concr. Compos. 94 (2018) 307–314, https://doi.org/10.1016/J.CEMCONCOMP.2018.10.002.

[79] H. Alghamdi, S.A.O. Nair, N. Neithalath, Insights into material design, extrusion rheology, and properties of 3D-printable alkali-activated fly ash-based binders, Mater. Des. 167 (2019) 107634, https://doi.org/10.1016/J.MATDES.2019.107634.

[80] H. Ilcan, O. Sahin, A. Kul, G. Yildirim, M. Sahmaran, Rheological properties and compressive strength of construction and demolition waste-based geopolymer mortars for 3D-Printing, Construct. Build. Mater. 328 (2022) 127114, https://doi.org/10.1016/J.CONBUILDMAT.2022.127114.

[81] N.C. Demiral, M. Ozkan Ekinci, O. Sahin, H. Ilcan, A. Kul, G. Yildirim, M. Sahmaran, Mechanical anisotropy evaluation and bonding properties of 3D-printable construction and demolition waste-based geopolymer mortars, Cem. Concr. Compos. 134 (2022) 104814, https://doi.org/10.1016/J.CEMCONCOMP.2022.104814.

[82] D. Chaiyotha, W. Kantawong, P. Payakanitia, S. Pinitsoontorn, P. Chindaprasirt, Finding optimized conditions for 3D printed high calcium fly ash based alkali-activated mortar, Case Stud. Constr. Mater. 18 (2023) e01976, https://doi.org/10.1016/J.CSCM.2023.E01976.

[83] R.J.M. Wolfs, F.P. Bos, T.A.M. Salet, Hardened properties of 3D printed concrete: the influence of process parameters on interlayer adhesion, Cement Concr. Res. 119 (2019) 132–140, https://doi.org/10.1016/J.CEMCONRES.2019.02.017.

[84] S. Yaseri, G. Hajiaghaei, F. Mohammadi, M. Mahdikhani, R. Farokhzad, The role of synthesis parameters on the workability, setting and strength properties of binary binder based geopolymer paste, Construct. Build. Mater. 157 (2017) 534–545, https://doi.org/10.1016/J.CONBUILDMAT.2017.09.102.

[85] P. Duxson, J.L. Provis, G.C. Lukey, S.W. Mallicoat, W.M. Kriven, J.S.J. Van Deventer, Understanding the relationship between geopolymer composition, microstructure and mechanical properties, Colloids Surf. A Physicochem. Eng. Asp. 269 (2005) 47–58, https://doi.org/10.1016/J.COLSURFA.2005.06.060.

[86] B.H.W.S. de Jong, G.E. Brown, Polymerization of silicate and aluminate tetrahedra in glasses, melts, and aqueous solutions—I. Electronic structure of H6Si2O7, H6AlSiO71−, and H6Al2O72, Geochem. Cosmochim. Acta 44 (1980) 491–511, https://doi.org/10.1016/0016-7037(80)90046-0.

[87] G. Kovalchuk, A. Fernández-Jiménez, A. Palomo, Alkali-activated fly ash: effect of thermal curing conditions on mechanical and microstructural development – Part II, Fuel 86 (2007) 315–322, https://doi.org/10.1016/J.FUEL.2006.07.010.

[88] M. Komljenović, Z. Baščarević, V. Bradić, Mechanical and microstructural properties of alkali-activated fly ash geopolymers, J. Hazard Mater. 181 (2010) 35–42, https://doi.org/10.1016/J.JHAZMAT.2010.04.064.

[89] S.W.M. Supit, M. Olivia, Compressive strength and sulfate resistance of metakaolin-based geopolymer mortar with different ratio of alkaline activator, Mater. Today Proc. 66 (2022) 2776–2779, https://doi.org/10.1016/j.matpr.2022.06.514.

[90] Z. Kubba, G. Fahim Huseien, A.R.M. Sam, K.W. Shah, M.A. Asaad, M. Ismail, M.M. Tahir, J. Mirza, Impact of curing temperatures and alkaline activators on compressive strength and porosity of ternary blended geopolymer mortars, Case Stud. Constr. Mater. 9 (2018), https://doi.org/10.1016/j.cscm.2018.e00205.

[91] R. Aurelie Tchouateu Kamwa, L. Tchadjie Noumbissie, S. Tome, E. Idriss, J. Giogetti Deutou Nemaleu, B. Tommes, D. Woschko, C. Janiak, M.A. Etoh, A comparative study of compressed lateritic earth bricks stabilized with natural pozzolan-based geopolymer binders synthesized in acidic and alkaline conditions, Construct. Build. Mater. 400 (2023), https://doi.org/10.1016/j.conbuildmat.2023.132652.

[92] K. Kaur, J. Singh, M. Kaur, Compressive strength of rice husk ash based geopolymer: the effect of alkaline activator, Construct. Build. Mater. 169 (2018) 188–192, https://doi.org/10.1016/j.conbuildmat.2018.02.200.

[93] M.N.S. Hadi, M. Al-Azzawi, T. Yu, Effects of fly ash characteristics and alkaline activator components on compressive strength of fly ash-based geopolymer mortar, Construct. Build. Mater. 175 (2018) 41–54, https://doi.org/10.1016/j.conbuildmat.2018.04.092.

[94] F. Gu, J. Xie, C. Vuye, Y. Wu, J. Zhang, Synthesis of geopolymer using alkaline activation of building-related construction and demolition wastes, J. Clean. Prod. 420 (2023), https://doi.org/10.1016/j.jclepro.2023.138335.

[95] Y. Yang, J. Zhang, Y. Fu, D. Hou, B. Dong, Alkaline hydrothermal activation of molybdenum tailings to prepare one-part geopolymer: activation mechanism and strength, J. Mater. Res. Technol. 25 (2023) 3789–3802, https://doi.org/10.1016/j.jmrt.2023.06.146.

[96] L. Kuang, G. Li, J. Xiang, W. Ma, X. Cui, Effect of seawater on the properties and microstructure of metakaolin/slag-based geopolymers, Construct. Build. Mater. 397 (2023), https://doi.org/10.1016/j.conbuildmat.2023.132418.

[97] Y. Luo, Z. Jiang, D. Wang, Y. Lv, C. Gao, G. Xue, Effects of alkaline activators on pore structure and mechanical properties of ultrafine metakaolin geopolymers cured at room temperature, Construct. Build. Mater. 361 (2022), https://doi.org/10.1016/j.conbuildmat.2022.129678.

[98] K. Bouguermouh, N. Bouzidi, L. Mahtout, L. Pérez-Villarejo, M.L. Martínez-Cartas, Effect of acid attack on microstructure and composition of metakaolin-based geopolymers: the role of alkaline activator, J. Non-Cryst. Solids 463 (2017) 128–137, https://doi.org/10.1016/j.jnoncrysol.2017.03.011.

[99] X. Zhang, J. Li, S. Pang, K. Zhu, L. Su, J. Liu, X. Zhang, Mechanical properties and interface microscopic characterisation of fibre-reinforced slag-fly ash geopolymer agglutinated iron tailings filling materials, Mater. Today Commun. 36 (2023), https://doi.org/10.1016/j.mtcomm.2023.106650.

[100] Z. Moujoud, S. Sair, H. Ait Ousaleh, I. Ayouch, A. El Bouari, O. Tanane, Geopolymer composites reinforced with natural Fibers: a review of recent advances in processing and properties, Construct. Build. Mater. 388 (2023), https://doi.org/10.1016/j.conbuildmat.2023.131666.

[101] M. Buyuktapu, M. Murat Maras, Optimization of production parameters of novel hybrid fiber-reinforced geopolymer mortar: application in masonry walls, Structures 53 (2023) 1300–1317, https://doi.org/10.1016/j.istruc.2023.05.031.

[102] K. Nazir, O. Canpolat, M. Uysal, Durability properties of steel, polyamide, and polyethylene fiber-reinforced geopolymer mortar made with recycled concrete aggregate and glass powder as fillers, J. Build. Eng. 76 (2023), https://doi.org/10.1016/j.jobe.2023.107313.

[103] A. Dhasmana, S. Singh, Long-term mechanical characteristics of fibre reinforced metakaolin-based geopolymer concrete: a review, Mater. Today Proc. (2023), https://doi.org/10.1016/j.matpr.2023.07.030.

[104] D. Zaharaki, K. Komnitsas, EFFECT OF ADDITIVES ON THE COMPRESSIVE STRENGTH OF SLAG-BASED INORGANIC POLYMERS, 2009.

[105] H. Xu, J.S.J. Van Deventer, The geopolymerisation of alumino-silicate minerals, Int. J. Miner. Process. 59 (2000) 247–266, https://doi.org/10.1016/S0301-7516(99)00074-5.

[106] T. Ding, J. Xiao, V. Mechtcherine, Microstructure and mechanical properties of interlayer regions in extrusion-based 3D printed concrete: a critical review, Cem. Concr. Compos. 141 (2023) 105154, https://doi.org/10.1016/J.CEMCONCOMP.2023.105154.

[107] H. Xu, J.S.J. Van Deventer, Geopolymerisation of multiple minerals, Miner. Eng. 15 (2002) 1131–1139, https://doi.org/10.1016/S0892-6875(02)00255-8.

[108] K. Chen, W.T. Lin, W. Liu, Microstructures and mechanical properties of sodium-silicate-activated slag/co-fired fly ash cementless composites, J. Clean. Prod. 277 (2020) 124025, https://doi.org/10.1016/J.JCLEPRO.2020.124025.

[109] K. Chen, W.T. Lin, W. Liu, Effect of NaOH concentration on properties and microstructure of a novel reactive ultra-fine fly ash geopolymer, Adv. Powder Technol. 32 (2021) 2929–2939, https://doi.org/10.1016/J.APT.2021.06.008.

[110] K. Chen, W.T. Lin, Q. Liu, B. Chen, V.W.Y. Tam, Micro-characterizations and geopolymerization mechanism of ternary cementless composite with reactive ultra-fine fly ash, red mud and recycled powder, Construct. Build. Mater. 343 (2022) 128091, https://doi.org/10.1016/J.CONBUILDMAT.2022.128091.

[111] F.A. Shilar, S.V. Ganachari, V.B. Patil, B.E. Bhojaraja, T.M. Yunus Khan, N. Almakayeel, A review of 3D printing of geopolymer composites for structural and functional applications, Construct. Build. Mater. 400 (2023) 132869, https://doi.org/10.1016/j.conbuildmat.2023.132869.

[112] M.B. Jaji, G.P.A.G. van Zijl, A.J. Babafemi, Slag-modified metakaolin-based geopolymer for 3D concrete printing application: evaluating fresh and hardened properties, Clean Eng Technol 15 (2023) 100665, https://doi.org/10.1016/j.clet.2023.100665.

[113] S. Muthukrishnan, S. Ramakrishnan, J. Sanjayan, Effect of microwave heating on interlayer bonding and buildability of geopolymer 3D concrete printing, Construct. Build. Mater. 265 (2020), https://doi.org/10.1016/j.conbuildmat.2020.120786.

[114] N.C. Demiral, M. Ozkan Ekinci, O. Sahin, H. Ilcan, A. Kul, G. Yildirim, M. Sahmaran, Mechanical anisotropy evaluation and bonding properties of 3D-printable construction and demolition waste-based geopolymer mortars, Cem. Concr. Compos. 134 (2022) 104814, https://doi.org/10.1016/J.CEMCONCOMP.2022.104814.

[115] E. Keita, H. Bessaies-Bey, W. Zuo, P. Belin, N. Roussel, Weak bond strength between successive layers in extrusion-based additive manufacturing: measurement and physical origin, Cement Concr. Res. 123 (2019) 105787, https://doi.org/10.1016/J.CEMCONRES.2019.105787.

[116] G.M. Moelich, J. Kruger, R. Combrinck, Modelling the interlayer bond strength of 3D printed concrete with surface moisture, Cement Concr. Res. 150 (2021) 106559, https://doi.org/10.1016/J.CEMCONRES.2021.106559.

[117] P. Tahmasebi, A state-of-the-art review of experimental and computational studies of granular materials: properties, advances, challenges, and future directions, Prog. Mater. Sci. 138 (2023) 101157, https://doi.org/10.1016/J.PMATSCI.2023.101157.

[118] K. Taj, H. İlcan, E. Teksin, G. Argın, M.K. Ardoğa, B. Uzal, M. Şahmaran, Effect of duration and type of grinding on the particle size distribution and microstructure of natural pumice with low pozzolanic reactivity, Powder Technol. 428 (2023) 118839, https://doi.org/10.1016/J.POWTEC.2023.118839.

[119] B. Panda, G.B. Singh, C. Unluer, M.J. Tan, Synthesis and characterization of one-part geopolymers for extrusion based 3D concrete printing, J. Clean. Prod. 220 (2019) 610–619, https://doi.org/10.1016/J.JCLEPRO.2019.02.185.

[120] S. Puligilla, P. Mondal, Role of slag in microstructural development and hardening of fly ash-slag geopolymer, Cement Concr. Res. 43 (2013) 70–80, https://doi.org/10.1016/J.CEMCONRES.2012.10.004.

[121] J. Temuujin, A. van Riessen, R. Williams, Influence of calcium compounds on the mechanical properties of fly ash geopolymer pastes, J. Hazard Mater. 167 (2009) 82–88, https://doi.org/10.1016/J.JHAZMAT.2008.12.121.
[122] C.K. Yip, G.C. Lukey, J.S.J. Van Deventer, The coexistence of geopolymeric gel and calcium silicate hydrate at the early stage of alkaline activation, Cement Concr. Res. 35 (2005) 1688–1697, https://doi.org/10.1016/J.CEMCONRES.2004.10.042.
[123] C.K. Yip, G.C. Lukey, J.L. Provis, J.S.J. van Deventer, Effect of calcium silicate sources on geopolymerisation, Cement Concr. Res. 38 (2008) 554–564, https://doi.org/10.1016/J.CEMCONRES.2007.11.001.
[124] M. Song, J. Qian, L.J. Zhong, S. Liang, From a view of alkali solution: alkali concentration to determine hydration process of alkali activating metakaolin, RILEM Bookseries 10 (2015) 305–313, https://doi.org/10.1007/978-94-017-9939-3_38.
[125] M. Rowles, B. O'Connor, Chemical optimisation of the compressive strength of aluminosilicate geopolymers synthesised by sodium silicate activation of metakaolinite, J. Mater. Chem. 13 (2003) 1161–1165, https://doi.org/10.1039/b212629j.
[126] J. Thaarrini, R. Venkatasubramani, Feasibility studies on compressive strength of ground coal ash geopolymer mortar, Period. Polytech. Civ. Eng. 59 (2015) 373–379, https://doi.org/10.3311/ppci.7696.
[127] S. Zhou, C. Lu, X. Zhu, F. Li, Preparation and characterization of high-strength geopolymer based on BH-1 lunar soil simulant with low alkali content, Engineering 7 (2021) 1631–1645, https://doi.org/10.1016/J.ENG.2020.10.016.
[128] U. Javed, F. Uddin Ahmed Shaikh, P. Kumar Sarker, Microstructural investigation of thermo-mechanically processed lithium slag for geopolymer precursor using various characterization techniques, Construct. Build. Mater. 342 (2022) 127952, https://doi.org/10.1016/J.CONBUILDMAT.2022.127952.
[129] F.J.H. Tommasini Vieira Ramos, M. de Fátima Marques Vieira, L.G.P. Tienne, V. de Oliveira Aguiar, Evaluation and characterization of geopolymer foams synthesized from blast furnace with sodium metasilicate, J. Mater. Res. Technol. 9 (2020) 12019–12029, https://doi.org/10.1016/J.JMRT.2020.08.019.
[130] T.C. Mahutjane, L.N. Tchadjié, T.N. Sithole, The feasibility of utilizing sewage sludge as a source of aluminosilicate to synthesise geopolymer cement, J. Mater. Res. Technol. 25 (2023) 3314–3323, https://doi.org/10.1016/J.JMRT.2023.06.116.
[131] E. Mahfoud, W. Maherzi, K. Ndiaye, M. Benzerzour, S. Aggoun, N.E. Abriak, Mechanical and microstructural properties of just add water geopolymer cement comprised of Thermo-Mechanicalsynthesis Sediments-Fly ash mix, Construct. Build. Mater. 400 (2023) 132626, https://doi.org/10.1016/J.CONBUILDMAT.2023.132626.
[132] I.O. Erunkulu, G. Malumbela, O.P. Oladijo, Feasibility of geopolymer synthesis using soda ash in copper slag blended fly ash-based geopolymer, Mater. Today Proc. 86 (2023) 41–46, https://doi.org/10.1016/J.MATPR.2023.02.208.
[133] A. Sharmin, U.J. Alengaram, M.Z. Jumaat, M.O. Yusuf, S.M.A. Kabir, I.I. Bashar, Influence of source materials and the role of oxide composition on the performance of ternary blended sustainable geopolymer mortar, Construct. Build. Mater. 144 (2017) 608–623, https://doi.org/10.1016/J.CONBUILDMAT.2017.03.178.
[134] N.H. Jamil, M.M. Al Bakri Abdullah, F.C. Pa, H. Mohamad, W.M.A.W. Ibrahim, J. Chaiprapa, Influences of SiO2, Al2O3, CaO and MgO in phase transformation of sintered kaolin-ground granulated blast furnace slag geopolymer, J. Mater. Res. Technol. 9 (2020) 14922–14932, https://doi.org/10.1016/J.JMRT.2020.10.045.
[135] I. Garcia-Lodeiro, A. Palomo, A. Fernández-Jiménez, D.E. MacPhee, Compatibility studies between N-A-S-H and C-A-S-H gels. Study in the ternary diagram Na2O–CaO–Al2O3–SiO2–H2O, Cement Concr. Res. 41 (2011) 923–931, https://doi.org/10.1016/J.CEMCONRES.2011.05.006.
[136] Y. Zhao, Y. Gao, G. Chen, S. Li, A. Singh, X. Luo, C. Liu, J. Gao, H. Du, Development of low-carbon materials from GGBS and clay brick powder for 3D concrete printing, Construct. Build. Mater. 383 (2023) 131232, https://doi.org/10.1016/J.CONBUILDMAT.2023.131232.
[137] M. Dabaieh, J. Heinonen, D. El-Mahdy, D.M. Hassan, A comparative study of life cycle carbon emissions and embodied energy between sun-dried bricks and fired clay bricks, J. Clean. Prod. 275 (2020) 122998, https://doi.org/10.1016/J.JCLEPRO.2020.122998.
[138] Q. Munir, M. Abdulkareem, M. Horttanainen, T. Kärki, A comparative cradle-to-gate life cycle assessment of geopolymer concrete produced from industrial side streams in comparison with traditional concrete, Sci. Total Environ. (2023) 865, https://doi.org/10.1016/j.scitotenv.2022.161230.
[139] N. Mir, S.A. Khan, A. Kul, O. Sahin, M. Sahmaran, M. Koc, Life cycle assessment of construction and demolition waste-based geopolymers suited for use in 3-dimensional additive manufacturing, Clean Eng Technol 10 (2022), https://doi.org/10.1016/j.clet.2022.100553.
[140] A. Kul, B.F. Ozel, E. Ozcelikci, M.F. Gunal, H. Ulugol, G. Yildirim, M. Sahmaran, Characterization and life cycle assessment of geopolymer mortars with masonry units and recycled concrete aggregates assorted from construction and demolition waste, J. Build. Eng. 78 (2023) 107546, https://doi.org/10.1016/j.jobe.2023.107546.
[141] F. Matalkah, P. Soroushian, Role of CO2 in enhancing geopolymer properties formulated with fluidized bed combustion ash, J. CO2 Util. 71 (2023) 102462, https://doi.org/10.1016/J.JCOU.2023.102462.
[142] A. Aziz, A. Bellil, I.E. El Amrani El Hassani, M. Fekhaoui, M. Achab, A. Dahrouch, A. Benzaouak, Geopolymers based on natural perlite and kaolinic clay from Morocco: synthesis, characterization, properties, and applications, Ceram. Int. 47 (2021) 24683–24692, https://doi.org/10.1016/J.CERAMINT.2021.05.190.
[143] G.L.V. Krishnam Raju, T. Vamsi Nagaraju, K. Jagadeep, M. Venkata Rao, V. Chanakya Varma, Waste-to-energy agricultural wastes in development of sustainable geopolymer concrete, Mater. Today Proc. (2023), https://doi.org/10.1016/J.MATPR.2023.05.481.
[144] Y. Shi, Q. Zhao, C. Xue, Y. Jia, W. Guo, Y. Zhang, Y. Qiu, Preparation and curing method of red mud-calcium carbide slag synergistically activated fly ash-ground granulated blast furnace slag based eco-friendly geopolymer, Cem. Concr. Compos. 139 (2023) 104999, https://doi.org/10.1016/J.CEMCONCOMP.2023.104999.
[145] J. Zhang, Y. Fu, A. Wang, B. Dong, Research on the mechanical properties and microstructure of fly ash-based geopolymers modified by molybdenum tailings, Construct. Build. Mater. 385 (2023) 131530, https://doi.org/10.1016/J.CONBUILDMAT.2023.131530.
[146] M.S.K. Chaitanya, T.V. Nagaraju, L.V.K.R. Gadhiraju, V.R. Madepalli, S. Narayana Raju Jampana, Strength and micro-structural performance of geopolymer concrete using highly burned rice husk ash, Mater. Today Proc. (2023), https://doi.org/10.1016/J.MATPR.2023.04.617.
[147] C. Ma, B. Zhao, S. Guo, G. Long, Y. Xie, Properties and characterization of green one-part geopolymer activated by composite activators, J. Clean. Prod. 220 (2019) 188–199, https://doi.org/10.1016/J.JCLEPRO.2019.02.159.
[148] J. Thaarrini, S. Dhivya, S. Dhivya, Comparative Study on the Production Cost of Geopolymer and Conventional Concretes, 2016. http://www.ripublication.com.
[149] R. Abbas, M.A. Khereby, H.Y. Ghorab, N. Elkhoshkhany, Preparation of geopolymer concrete using Egyptian kaolin clay and the study of its environmental effects and economic cost, Clean Technol. Environ. Policy 22 (2020) 669–687, https://doi.org/10.1007/s10098-020-01811-4.
[150] G. Chen, D. ping Zheng, Y. wu Chen, J.X. Lin, W. jian Lao, Y. chang Guo, Z. biao Chen, X. wei Lan, Development of high performance geopolymer concrete with waste rubber and recycle steel fiber: a study on compressive behavior, carbon emissions and economical performance, Construct. Build. Mater. 393 (2023) 131988, https://doi.org/10.1016/J.CONBUILDMAT.2023.131988.
[151] J. Zhao, J. Xie, J. Wu, C. Zhao, B. Zhang, Workability, compressive strength, and microstructures of one-part rubberized geopolymer mortar, J. Build. Eng. 68 (2023) 106088, https://doi.org/10.1016/J.JOBE.2023.106088.
[152] M. He, Z. Yang, N. Li, X. Zhu, B. Fu, Z. Ou, Strength, microstructure, CO2 emission and economic analyses of low concentration phosphoric acid-activated fly ash geopolymer, Construct. Build. Mater. 374 (2023) 130920, https://doi.org/10.1016/J.CONBUILDMAT.2023.130920.
[153] M. Refaat, A. Mohsen, E.S.A.R. Nasr, M. Kohail, Minimizing energy consumption to produce safe one-part alkali-activated materials, J. Clean. Prod. 323 (2021) 129137, https://doi.org/10.1016/J.JCLEPRO.2021.129137.
[154] R. Mohana, S.M. Leela Bharathi, Sustainable utilization of pre-treated and nano fly ash powder for the development of durable geopolymer mortars, Adv. Powder Technol. 33 (2022) 103696, https://doi.org/10.1016/J.APT.2022.103696.
[155] A. Danish, A. Öz, B. Bayrak, G. Kaplan, A.C. Aydın, T. Ozbakkaloglu, Performance evaluation and cost analysis of prepacked geopolymers containing waste marble powder under different curing temperatures for sustainable built environment, Resour. Conserv. Recycl. 192 (2023) 106910, https://doi.org/10.1016/J.RESCONREC.2023.106910.
[156] Q. Zhao, C. Ma, B. Huang, X. Lu, Development of alkali activated cementitious material from sewage sludge ash: two-part and one-part geopolymer, J. Clean. Prod. 384 (2023) 135547, https://doi.org/10.1016/J.JCLEPRO.2022.135547.

[157] Y. Li, J. Shen, H. Lin, Y. Li, Optimization design for alkali-activated slag-fly ash geopolymer concrete based on artificial intelligence considering compressive strength, cost, and carbon emission, J. Build. Eng. 75 (2023) 106929, https://doi.org/10.1016/J.JOBE.2023.106929.
[158] Geoffrey Hammond, Craig Jones, Fiona Lowrie, Peter Tse, Building Services Research and Information Association., University of Bath., Embodied Carbon : the Inventory of Carbon and Energy (ICE), BSRIA, 2011.
[159] S. Bhattacherjee, A.S. Basavaraj, A.V. Rahul, M. Santhanam, R. Gettu, B. Panda, E. Schlangen, Y. Chen, O. Copuroglu, G. Ma, L. Wang, M.A. Basit Beigh, V. Mechtcherine, Sustainable materials for 3D concrete printing, Cem. Concr. Compos. 122 (2021) 104156, https://doi.org/10.1016/J.CEMCONCOMP.2021.104156.
[160] M.M. El-Attar, D.M. Sadek, A.M. Salah, Recycling of high volumes of cement kiln dust in bricks industry, J. Clean. Prod. 143 (2017) 506–515, https://doi.org/10.1016/J.JCLEPRO.2016.12.082.
[161] B. Kanagaraj, N. Anand, R. Samuvel Raj, E. Lubloy, Techno-socio-economic aspects of Portland cement, geopolymer, and limestone calcined clay cement (LC3) composite systems: a-state-of-art-review, Construct. Build. Mater. 398 (2023) 132484, https://doi.org/10.1016/J.CONBUILDMAT.2023.132484.
[162] Y.L. Li, M.Y. Han, S.Y. Liu, G.Q. Chen, Energy consumption and greenhouse gas emissions by buildings: a multi-scale perspective, Build. Environ. 151 (2019) 240–250, https://doi.org/10.1016/J.BUILDENV.2018.11.003.
[163] H. Mikulčić, J.J. Klemeš, M. Vujanović, K. Urbaniec, N. Duić, Reducing greenhouse gasses emissions by fostering the deployment of alternative raw materials and energy sources in the cleaner cement manufacturing process, J. Clean. Prod. 136 (2016) 119–132, https://doi.org/10.1016/J.JCLEPRO.2016.04.145.
[164] J. Zhang, D. Peng, X. Gao, J. Zou, L. Ye, G. Ji, B. Luo, G. Yu, P. Li, X. Wang, Z. Zhao, B. Zhang, W. Hu, Z. Liu, L. Cheng, R. Zhao, Regeneration of high-performance materials for electrochemical energy storage from assorted solid waste: a review, J. Clean. Prod. 416 (2023) 137628, https://doi.org/10.1016/J.JCLEPRO.2023.137628.